Inorganic Chemistry

Article

pubs.acs.org/IC

Synthesis, Characterization, and Electron-Transfer Processes in Indium Ferrocenyl-Containing Porphyrins and Their Fullerene Adducts

Samantha J. Dammer, Pavlo V. Solntsev, Jared R. Sabin, and Victor N. Nemykin*

Department of Chemistry and Biochemistry, University of Minnesota Duluth, 1039 University Drive, Duluth, Minnesota 55812, United States

Supporting Information

ABSTRACT: Three new indium(III) tetra- and penta-(ferrocenyl)-substituted porphyrins of the general formula XInTFcP [X = Cl^-, OH^-, or Fc^-; TFcP = 5,10,15,20-tetraferrocenylporphyrin(2-); Fc = ferrocene] have been prepared and characterized by UV−vis, magnetic circular dichroism (MCD), ^1H, ^{13}C, 2D, and variable-temperature NMR spectroscopy, as well as elemental analysis. Molecular structures of the ClInTFcP, FcInTFcP, and FcInTFcP@4C_{60} complexes were determined by X-ray crystallography with the last compound being not only the first example of a C_{60} adduct to the organometallic porphyrins but also the first structure in which organometallic porphyrin antennas intercalated into four electron-transfer channels. The electronic structures and relative energies of individual atropisomers, as well as prospective electron-transfer properties of fullerene adducts of XInTFcP complexes, were investigated by the Density Functional Theory (DFT) approach. Redox properties of XInTFcP complexes were investigated using electrochemical (CV and DPV), spectroelectrochemical, and chemical oxidation approaches. Electrochemical experiments conducted in low-polarity solvent using noncoordinating electrolyte were crucial for the sequential oxidation of ferrocene substituents in XInTFcP compounds. In agreement with DFT calculations, the axial ferrocene ligand in FcInTFcP, with direct In−C σ-bond has a 240 mV lower oxidation potential compared to the first oxidation potential for equatorial ferrocene substituents connected to the porphyrin core. The first equatorial ferrocene oxidation process in all XInTFcP complexes is separated by at least 150 mV from the next three ferrocene based oxidations. The second, third, and fourth redox processes in the ferrocene region are more closely spaced. The addition of the bulky axial ferrocene ligand results in significantly larger rotational barriers for equatorial ferrocene substituents in FcInTFcP compared to the other complexes and leads to better defined redox waves in cyclic voltammetry (CV) and differential pulse voltammetry (DPV) experiments. Mixed-valence compounds of the general formula $[XInTFcP]^{n+}$ (n = 1, 2) were observed and characterized by spectroelectrochemical and chemical oxidation approaches. In all cases, the presence of the intense intervalence charge transfer (IVCT) bands associated with the oxidation of a single equatorial ferrocene substituent were detected in the NIR region confirming the presence of the iron-based mixed-valence species and suggesting long-range metal−metal coupling in the target systems. The resulting data from the mixed-valence $[XInTFcP]^{n+}$ (n = 1, 2) complexes matched very closely to the previously reported MTFcP and metal-free poly(ferrocenyl)porphyrins and were assigned as Robin and Day Class II mixed-valence compounds.

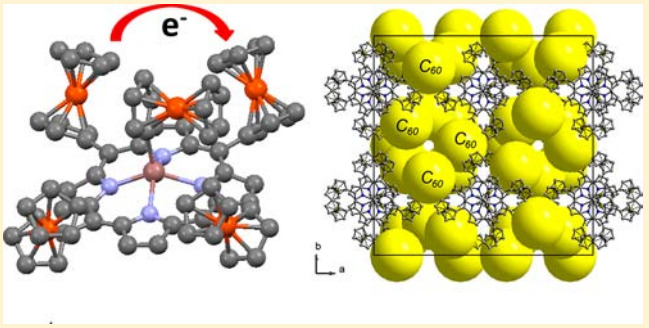

INTRODUCTION

Organometallic donor−acceptor assemblies with tunable electron-transfer and strong visible light absorption properties were intensively studied as perspective light-harvesting antennae for dye-sensitized solar cells (DSSCs) and organic photovoltaics (OPVs).[1] Poly(ferrocenyl)-containing compounds which exhibit strong metal−metal coupling were suggested as potentially useful components for molecular electronics and optical limiting.[2] Ferrocenyl-containing tetraazaporphyrins,[4] phthalocyanines,[3] corroles,[5] and especially porphyrins[6−9] received a considerable attention because of their rich redox chemistry and redox-dependent spectroscopic versatility. Formation, stability, and electron-migration properties of the corresponding mixed-valence compounds raised particular interest in such compounds. The mixed-valence poly(ferrocenyl)-containing macrocycles were suggested as candidates for use in molecular electronics including, among other things, multibit information storage devices as well as redox-switchable optical and fluorescent elements active in the NIR region.[10] Metal-free and transition-metal poly(ferrocenyl)-containing porphyrins with ferrocene substituents directly connected to the porphyrin core via *meso*-carbon atoms, have recently been well characterized and were found to form mixed-

Received: May 9, 2013
Published: August 6, 2013

dx.doi.org/10.1021/ic401163y | *Inorg. Chem.* 2013, 52, 9496−9510

Scheme 1. Synthetic Pathways for Preparation of the XInTFcP Complexes

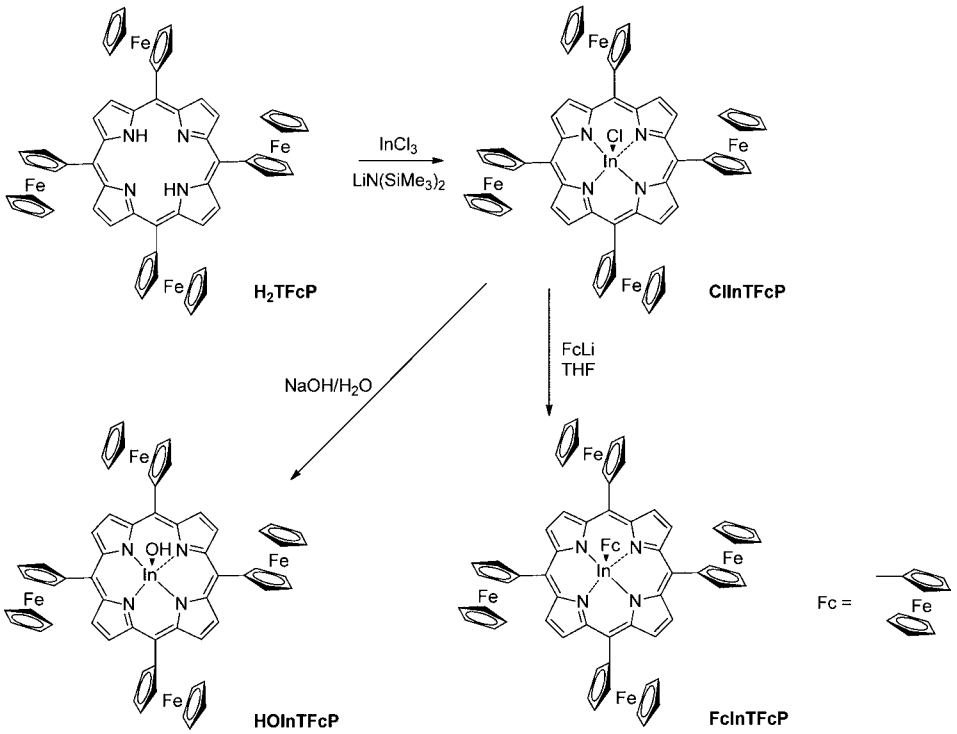

valence species upon chemical or electrochemical oxidations.[6h,j,l,m,o,q,r,7d]

In addition, porphyrins are well-known for their ability to form adducts with the classic electron-acceptors such as fullerene and its derivatives[11,12] in which porphyrin core acts as a light-harvesting antenna and electron donor, while fullerene works as electron acceptor to form a charge-separation state. Formation of such a charge-separation state is a key for efficient light-harvesting and light-to-current energy conversion in porphyrin-fullerene assemblies. It has been shown that the addition of a terminal ferrocene donor to the covalently linked porphyrin-fullerene assembly results in significantly longer lifetime of charge-separation states, which results in more efficient light-to-current conversion.[13] Noncovalent ferrocene-porphyrin to fullerene assemblies, however, have not been intensively targeted despite their lower cost, easiness in preparation, and potential usefulness in organic photovoltaics. Such noncovalent supramolecular assembly formation requires fine-tuning of the electron density in ferrocene-porphyrin donor-antenna unit. In the case of ferrocene-porphyrins with direct ferrocene to porphyrin bonds, electron density could be modulated by the central metal. Thus, according to the density functional theory (DFT) calculations and available single-crystal X-ray data, introduction of a central metal into the porphyrin cavity results in a change of the degree of nonplanarity of the porphyrin core,[6o,r,7d] which could potentially affect the extent of the metal−metal interactions in these systems. In addition, central metal based orbitals may influence electron-transfer pathway. Finally, a central metal could be used to link a macrocycle to a surface when the application to molecular electronics is the final goal.[6s] Except a single class of the double-decker diferrrocenylporphyrin-phthalocyanine compounds, all poly(ferrocenyl)-containing complexes published so far[14] have a central metal located in the porphyrin N4 cavity, while the redox properties of the tetraferrocenyl-containing porphyrins (MTFcP) with an "out-of-plane" located central ion remains unexplored. Moreover, an intercalation of the poly(ferrocene)-containing porphyrins into the fullerene matrix has never been reported. To investigate an influence of the out-of-plane central atom in MTFcP complexes on their redox behavior and explore the possibility of the axial functionalization, we have prepared and characterized the series of XInTFcP (X = Cl^-, OH^-, or Fc^-) complexes (Scheme 1). We have also investigated cocrystallization of new potentially light-harvesting organometallic donor-porphyrin antenna dyads with the classic electron-acceptor (fullerene) to explore potential application of ferrocene-containing porphyrins in organic photovoltaics.

RESULTS AND DISCUSSION

Synthesis of XInTFcP Complexes. A standard synthetic route for preparation of the indium(III) porphyrins requires heating of the metal-free porphyrin and indium(III) salt or oxide in the glacial acetic acid or melted phenol media for long periods of time.[15] Our initial attempts to prepare the target ClInTFcP complex using such standard approaches failed because of the well-known oxidative decomposition of the ferrocenyl-containing porphyrins in acidic media or at high temperatures. Thus, because of the acid sensitivity of the ferrocene substituents present in the parent H_2TFcP compound, we developed a new method for the preparation of the ClInTFcP, similar to that used in synthesis of indium chlorines[16] (Scheme 1). In this approach, H_2TFcP complex was first deprotonated using $LiN(SiMe_3)_2$ and then reacted with $InCl_3$ in dry boiling tetrahydrofuran (THF) as a solvent (yield 52%). A substitution of the axial chloride anion by a hydroxo-group could be achieved in a low yield following procedure described earlier by Meyerhoff and co-workers.[17] In particular, washing a dichloromethane (DCM) solution of the ClInTFcP complex several times with cold 2 M NaOH and distilled water,

dx.doi.org/10.1021/ic401163y | Inorg. Chem. 2013, 52, 9496−9510

Table 1. Summary of Crystallographic Data for the ClInTFcP and FcInTFcP Complexes

	ClInTFcP	FcInTFcP	FcInTFcP@4C_{60}
empirical formula	$C_{70.90}H_{62.75}N_4ClFe_4In$	$C_{70}H_{53}N_4Fe_5In$	$C_{310}H_{53}Fe_5N_4In$
formula weight	1344.47	1344.23	4226.63
crystal system	triclinic	triclinic	tetragonal
space group, Z	$P\bar{1}$, 2	$P\bar{1}$, 2	$I4_1/acd$, 8
a (Å)	11.2415(3)	13.7094(6)	36.8912(7)
b (Å)	15.3866(3)	14.5527(9)	36.8912(7)
c (Å)	16.2741(11)	15.8180(11)	24.7083(17)
α (deg)	82.613(6)	69.953(5)	90
β (deg)	81.185(6)	76.118(5)	90
γ (deg)	76.854(5)	63.423(5)	90
volume (Å^3)	2695.9(2)	2637.3(3)	33627(3)
ρ_{calc} (g/cm^3)	1.656	1.693	1.670
μ(mm^{-1})	1.573	1.820	0.637
θ_{max} (deg)	27.48	25.04	26.372
meas./unique reflns	73246/12287	26966/9252	44013/8438
R_{int}	0.0380	0.0879	0.0237
GoF (F^2)	1.131	1.010	1.905
R_1, wR_2 ($I > 2\sigma(I)$)	0.0391[a], 0.0965[b]	0.0549[a], 0.1274[b]	0.1134[a], 0.3777[c]
R_1, wR_2 (all data)	0.0437[a], 0.0986[b]	0.0810[a], 0.1435[b]	0.1197[a], 0.3848[c]
$\Delta\rho_{max}/\Delta\rho_{min}$ (e/Å^3)	0.595/−0.450	1.171/−0.953	3.903/-1.675

[a] $R_1(F) = \sum||F_o| - |F_c||/\sum|F_o|$. [b] $wR_2(F^2) = \{\sum[w(F_o^2 - F_c^2)^2]/\sum w(F_o^2)^2]\}^{1/2}$. [c] $w = 1/[\sigma^2(F_o^2) + (3/5(F_o^2 + 2F_c^2))^2]$.

Table 2. Selected Bond Lengths (Å) and Angles (deg) for the ClInTFcP and FcInTFcP Complexes

	ClInTFcP		
In(1A)−N(1)	2.146(2)	N(1)−In(1A)−N(4)	85.75(9)
In(1A)−N(4)	2.153(2)	N(1)−In(1A)−N(2)	86.70(9)
In(1A)−N(2)	2.158(2)	N(4)−In(1A)−N(2)	150.45(10)
In(1A)−N(3)	2.171(3)	N(1)−In(1A)−N(3)	147.85(10)
In(1A)−Cl(1A)	2.3940(10)	N(4)−In(1A)−N(3)	85.80(9)
N(1)−In(1A)−Cl(1A)	99.30(8)	N(2)−In(1A)−N(3)	85.55(9)
N(4)−In(1A)−Cl(1A)	103.94(8)	N(2)−In(1A)−Cl(1A)	105.46(8)
Fe···π^a(centroid)	1.658(2), 1.653(2), 1.647(2), 1.645(2), 1.656(2), 1.655(2), 1.659(2), 1.656(2)	Fe···C(average)	2.049(3)
	FcInTFcP		
In(1)−C(61)	2.152(6)	C(61)−In(1)−N(2)	106.3(2)
In(1)−N(3)	2.183(4)	C(61)−In(1)−N(4)	112.3(2)
In(1)−N(1)	2.191(4)	N(3)−In(1)−N(1)	138.43(16)
In(1)−N(4)	2.213(4)	N(3)−In(1)−N(4)	83.41(16)
In(1)−N(2)	2.218(4)	N(1)−In(1)−N(4)	83.23(15)
C(61)−In(1)−N(3)	113.85(19)	N(3)−In(1)−N(2)	82.97(16)
C(61)−In(1)−N(1)	107.65(19)	N(1)−In(1)−N(2)	83.41(16)
		N(4)−In(1)−N(2)	141.35(16)
Fe···π^b(centroid)	1.656(3), 1.663(4) 1.661(4), 1.664(5) 1.659(3), 1.653(3) 1.650(3), 1.659(3) 1.650(4), 1.659(4)	Fe···C(average)	2.048(8)
	FcInTFcP@4C_{60}		
In11−C161	2.205(13)	C161−In11−N11	112.83(12)
In11−N11	2.231(5)	N11−In11−N11[c]	134.3(2)
Fe···C(average)	2.048(8)	C41−C51−C61−C101	130.5(5)
Fe···π^d(centroid)	1.657(2), 1.657(2), 1.645(13)		

[a] Ring centroids were built on C21−C22−C23−C24−C25, C26−C27−C28−C29−C30, C31−C32−C33−C34−C35, C36−C37−C38−C39−C40, C41−C42−C43−C44−C45, C46−C47−C48−C49−C50, C51−C52−C53−C54−C55, and C56−C57−C58−C59−C60. [b] Ring centroids were built on C21−C22−C23−C24−C25, C26−C27−C28−C29−C30, C31−C32−C33−C34−C35, C36−C37−C38−C39−C40, C41−C42−C43−C44−C45, C46−C47−C48−C49−C50, C51−C52−C53−C54−C55, C56−C57−C58−C59−C60, C61−C62−C63−C64−C65 and C66−C67−C68−C69−C70. [c] 1−x, 1/2−y, z. [d] Ring centroids were built on C6−C7−C8−C9−C10, C11−C12−C13−C14−C15, C21−C22−C23−C24−C25.

followed by removal of organic solvent and recrystallization from DCM/hexanes afforded the HOInTFcP complex in 14% yield. Again, all our attempts to exchange the axial chloride in ClInTFcP using hydrolysis at elevated temperatures resulted in formation of a black insoluble residue that was not further characterized. Because of the low yield of the HOInTFcP

dx.doi.org/10.1021/ic401163y | Inorg. Chem. 2013, 52, 9496−9510

complex, we did not further investigate its possible axial functionalization. Finally, the FcInTFcP complex was prepared in a good yield by reaction between ClInTFcP and ferrocene-lithium salt following a procedure published by us earlier for axial functionalization of Cl_2SnTPP (TPP(2-) is a dianion of 5,10,15,20-tetraphenylporphyrin) complexes.[9b] It should be noted, that to the best of our knowledge, the FcInTFcP complex is the first organometallic porphyrin with *both* axial and equatorial σ-bonded ferrocenyl groups directly bounded to the porphyrin core.

X-ray Crystal Structures. An ultimate knowledge on the chemical structures of ClInTFcP and FcInTFcP was further gained from the single-crystal X-ray analysis. Refinement parameters for the ClInTFcP and FcInTFcP complexes are presented in Table 1, their selected bonds lengths and angles are summarized in Table 2, and ORTEP diagrams are shown in Figures 1 and 2. In both structures, the indium ion has a

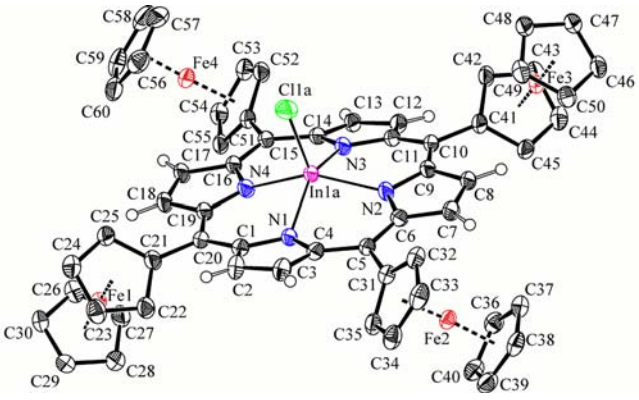

Figure 1. ORTEP diagram for the ClInTFcP complex. All hydrogen atoms are omitted for clarity. Thermal ellipsoids are at 50% probability.

tetragonal pyramidal geometry, which consists of four nitrogen atoms of the porphyrin core and a single axial ligand. The presence of a bulky axial ferrocene group in FcInTFcP leads to several significant deviations in geometry of the indium ion compared to the structure of ClInTFcP. First, the central indium ion is located further from the porphyrin N4 plane in FcInTFcP (0.755(1) Å) compared to ClInTFcP (0.574(1) Å). Second, the corresponding In−N bond distances are longer for the FcInTFcP complex (2.183(4)−2.218(4) Å) compared to ClInTFcP (2.146(2)−2.171(2) Å). The effect of the bulky axial ferrocene group also results in an asymmetry of the coordination environment of the indium ion. The interaction of the ferrocene group with porphyrin core leads to increase of the C(61)−In(1)−N(3) angles to 113.85(19)°, compared to C(61)−In(1)−N(1) angle (Table 2). Such an imbalance was not observed in ClInTFcP. The axial In−Cl distance in ClInTFcP is 2.394(1) Å, which is comparable to the distances observed for similar compounds (2.369(2),[18] 2.374(1) Å,[19] and 2.360(2) Å[20]). The axial In−C bond distance in FcInTFcP is 2.152(6) Å and is very close to that observed in a CH_3InTPP complex (2.1328(2) Å).[21] Unlike distorted H_2TFcP[6o] and ZnTFcP[7d] complexes that were reported earlier, both ClInTFcP and FcInTFcP complexes have quite a planar porphyrin core, and such a situation has recently been observed in the case of the $Cl_2SnTFcP$ compound.[6r] The axial ferrocene group in the FcInTFcP complex is almost coplanar with the N2−In1−N4 plane (torsion angle is 11.33°). All ferrocene

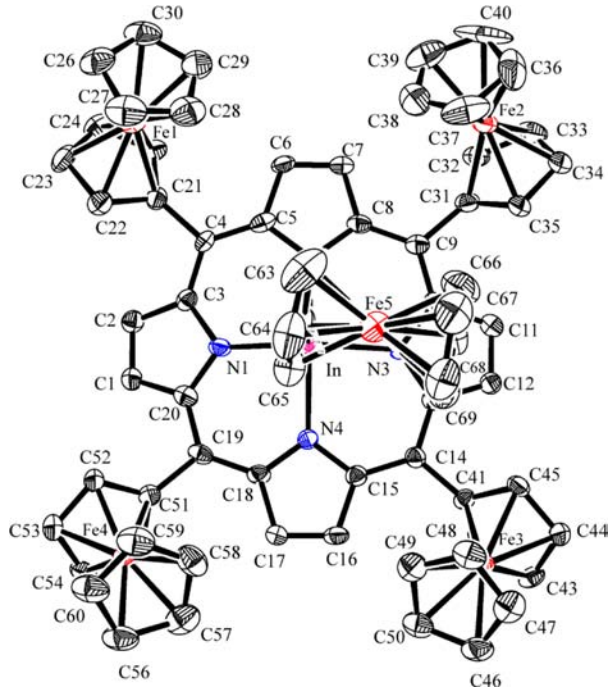

Figure 2. ORTEP diagram for the FcInTFcP complex. All hydrogen atoms are omitted for clarity. Thermal ellipsoids are at 50% probability.

substituents in the crystal structures of ClInTFcP and FcInTFcP were observed in an eclipsed conformation.

The ferrocene substituents in the ClInTFcP complex adopt an $\alpha,\alpha,\beta,\beta$ conformation similar to that observed in $Cl_2SnTFcP$ compound.[6r] In analogy with the $Cl_2SnTFcP$ compound, the reason for such a conformation is the presence of solvent molecules (toluene) in the crystal structure of the ClInTFcP complex (Figure 3). To accommodate the solvent molecule,

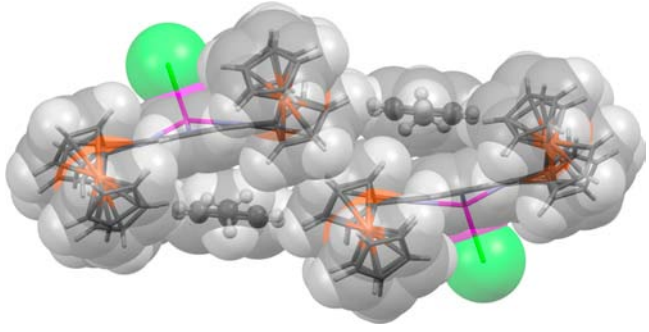

Figure 3. Packing diagram for the ClInTFcP complex.

ClInTFcP complexes form a zigzag structure with two ferrocene substituents adopting α,α and the other two ferrocene substituents adopting β,β conformations. Such an asymmetric zigzag motif creates solvent cavities large enough to accommodate the toluene solvent molecule, which can form effective $\pi-\pi$ interactions with the porphyrin core (Figure 3). The equatorial ferrocene substituents in the FcInTFcP complex have an unprecedented $\alpha,\alpha,\alpha,\alpha$ conformation (Figure 2), which, according to the DFT calculations presented below, is slightly energetically more favorable compared to the other atropisomers. An additional reason for such a conformation in the solid state is a strong $\pi-\pi$ interaction between two

dx.doi.org/10.1021/ic401163y | Inorg. Chem. 2013, 52, 9496−9510

neighboring porphyrin cores (Figure 4). In addition, similar $\pi-\pi$ ineractions exist between Cp rings of axial and equatorial σ-bonded ferrocenes (Cp_{axial}-$Cp_{equatorial}$ = 3.370 Å).

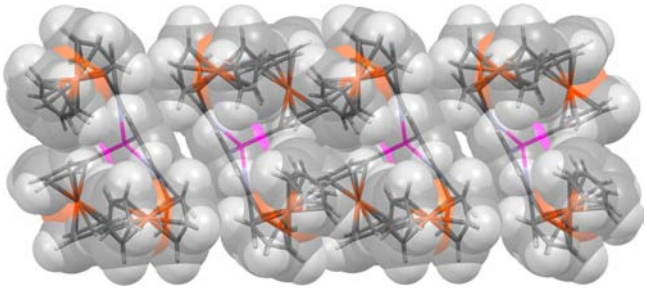

Figure 4. Packing diagram for the FcInTFcP complex.

NMR Spectroscopy. All indium complexes reported here differ only by the axial substituent, and thus the NMR spectra of the tetraferrocenyl-porphyrin fragment are close to each other and consist of the β-pyrrolic and three ferrocene-associated signals (Supporting Information, Figures S1–S8). In addition, the proton signal of the axial hydroxyl ligand in HOInTFcP was observed at −5.37 ppm because of the strong ring current created by the π-system of the porphyrin core. Similarly, proton signals for the axial ferrocene substituent in FcInTFcP were also significantly shifted upfield because of the porphyrin ring current as confirmed by COSY analysis. In each compound's ^{1}H NMR spectra, the three separate signals appearing for the ferrocene substituent, (α-Cp, β-Cp, and Cp-H protons) confirm that the ferrocene substituents are free to rotate around single C_{ipso}–C_{meso} bonds and probably adopt different conformations in the solid state as a result of different crystal packing interactions. It is also important to note that ClInTPP porphyrin does not reveal such behavior and has split signals of the ortho- protons of the phenyl ring.[18]

Taking into consideration a large difference in steric properties of the axial substituents in ClInTFcP and FcInTFcP complexes, we used variable temperature NMR spectroscopy to examine the barrier of rotation for the equatorial ferrocene substituents (Supporting Information, Figures S9 and S10). The activation barrier for rotation of the equatorial ferrocene substituents in the FcInTFcP complex was estimated to be 35.7 kJ/mol based on the coalescence temperature for β-protons in this compound. The smaller size of the axial chloride in the ClInTFcP complex leads to a significantly lower rotation barrier for the ferrocene substituents, which was roughly estimated to be smaller than 12.6 kJ/mol with a coalescence temperature below the freezing point of the solvent. Previous work with both tetraphenyl porphyrins[22] and tetraferrocenyl porphyrins[6l,7d] showed that the rotational barrier depends on the central metal ion.[22] Estimated activation energies for previously prepared tetraferrocenyl porphyrins increase in the order of Ni < H_2 < Zn[6l] When compared with the indium metalated porphyrins reported here, the compounds fall in the following order: InCl < Ni <H_2 < Zn < InFc. A relatively high rotational barrier observed in the case of the FcInTFcP complex can be easily attributed to the size of the axial ferrocene ligand.

UV–vis–NIR and MCD Spectra of XInTFcP Complexes. The UV–vis–NIR and magnetic circular dichroism (MCD) spectra of XInTFcP complexes are presented in Figure 5. Each UV–vis spectrum exhibits an intense Soret band located at 437–443 nm and a single Q-Band between 712 and 724 nm.

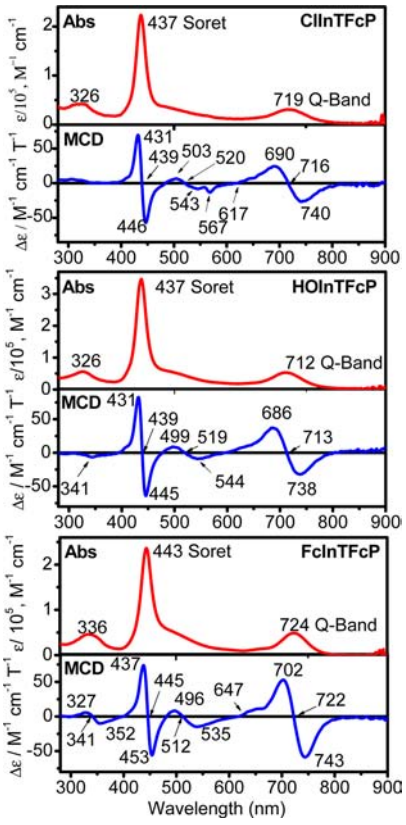

Figure 5. UV–vis–NIR and MCD spectra of ClInTFcP (top), HOInTFcP (middle), and FcInTFcP (bottom) complexes.

The Soret and Q-bands are correlate with Faraday A terms in the corresponding MCD spectra. The consistency of MCD Faraday A-terms in Soret- and Q-band regions found among all three indium compounds indicates that all three new compounds exhibit degeneracy in their excited state, which is consistent with effective C_{4v} symmetry. Since indium ion is located significantly out of the porphyrin N4 plane in XInTFcP complexes, an influence of the axial ligand on energies of excited states is significantly smaller compared to an influence of the axial ligands in recently reported Cl_2SnTPP and Fc_2SnTPP complexes (Sn(IV) ion is in N4 porphyrin plane).[9b] Indeed, both Soret and Q-bands in the FcInTFcP complex are shifted by ~5 nm to the lower energies from the Soret and Q-bands observed in complexes XInTFcP (X = Cl^- or OH^-), while an ~20 nm red shift was observed for the Soret and Q-bands when axial chlorine ligands in Cl_2SnTPP were replaced by ferrocene substituents.[9b]

Redox Properties of XInTFcP Complexes. Similar to the metal-free and transition-metal tetraferrocenyl porphyrins described earlier,[6h,m,o,q,7d] the redox properties of XInTFcP complexes were first evaluated using cyclic voltammetry (CV), differential pulse voltammetry (DPV), and square wave voltammetry (SWV) approaches. To minimize solute-electrolyte ion-pairing and thus improve the resolution between redox processes, all electrochemical and spectroelectrochemical were conducted using DCM as a solvent and, as suggested by Geiger and co-workers,[23] tetrabutylammonium tetrakis-(perfluorophenyl)borate (TBAF) as the electrolyte. CV and DPV results for all XInTFcP compounds are shown in Figure 6, while redox potentials are listed in Table 3.

dx.doi.org/10.1021/ic401163y | Inorg. Chem. 2013, 52, 9496–9510

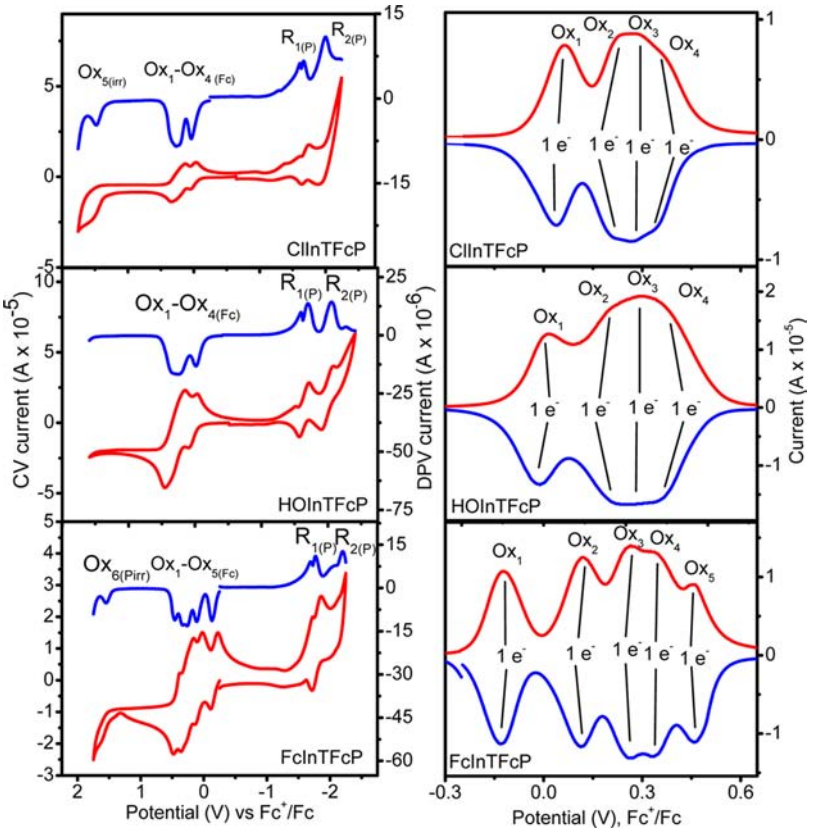

Figure 6. Electrochemical (CV and DPV) data on XInTFcP complexes in DCM/0.05 M TBAF system. Insets on the right side panels represent DPV data for the ferrocene substituents' oxidation only.

Table 3. Redox Potentials in Volts (versus Fc/Fc^+ Couple) of XInTFcP Complexes Determined in DCM/TBAF System[a]

porphyrin-centered reduction		ferrocene-centered oxidation					porphyrin-centered oxidation
P−2	P−1	Fc+1	Fc+2	Fc+3	Fc+4	Fc+5	P+1
			ClInTFcP				
−2.02	−1.68	0.06	0.22	0.28	0.36		1.48[irr]
			HOInTFcP				
−2.06	−1.70	0.02	0.20	0.32	0.42		
			FcInTFcP				
−2.2	−1.77	−0.13	0.11	0.26	0.35	0.46	1.55[irr]

[a]Abbreviations: P−1 and P−2 are first and second porphyrin-centered reductions, respectively; P+1 is a first porphyrin-centered oxidation; Fc +1−Fc+5 are respective ferrocene-centered oxidations. In all cases, when redox waves were closely spaced, their potentials were determined using DPV data deconvolution analysis.

In agreement with redox data on H_2TFcP, MTFcP (M = Co(II), Ni(II), Cu(II), Zn(II)), and Cl_2SnTFcP complexes,[6m,q,r] redox processes in XInTFcP complexes could be associated with oxidation of ferrocene substituents and oxidation/reduction of the porphyrin core. CV data suggest that both porphyrin-centered reductions observed between −1.6 and −2.4 V are reversible, while (if observed within electrochemical window) the porphyrin-centered oxidation process observed at ∼+1.5 V is irreversible. Oxidation of the ferrocene substituents in ClInTFcP and HOInTFcP complexes resemble the respective processes in H_2TFcP and MTFcP complexes.[6m,q,r] In particular, (i) each ferrocene substituent has an individual oxidation potential; (ii) the first oxidation potential is well separated (160−180 mV) from the other three processes; (iii) oxidation potentials of the remaining three ferrocene substituents are closely spaced, such that exact positions could only be determined by deconvolution analysis (Supporting Information, Figure S11); (iv) four ferrocene-centered oxidation processes span over a 300−400 mV range.

We were also curious to see how the 3-fold increase of the rotational barrier in the more sterically crowded FcInTFcP complex compared to ClInTFcP would affect the span and resolution of ferrocene-centered electrochemical waves. It has been mentioned earlier that rotational hindrance for the ferrocene-group rotation can cause a significant difference in the redox-behavior of poly(ferrocenyl)-containing porphyrins. Indeed, potentials for the first and second ferrocene oxidations in 5,15-bis(ferrocenyl)-10,20-diphenylporphyrin (with a low rotational barrier for the ferrocene groups) are separated by only 150 mV (DCM/TBAF system),[6o] while those for sterically crowded *α,α*-5,15-bis(ferrocenyl)-2,8,12,18-tetrabutyl-3,7,13,17-tetramethylporphyrin (with ferrocene groups locked in a single *α,α*-conformation) are separated by amazing 400 mV (DCM/TBAP system).[6c] Both CV and DPV data for the FcInTFcP complex (Figure 6) in the area of the ferrocene groups' oxidation clearly indicate five distinct processes associated with stepwise oxidation of individual ferrocene substituents. The lowest oxidation couple was observed at −130 mV versus the Fc/Fc^+ couple. This process is well-separated (240 mV) from remaining four waves. The second oxidation wave was observed at +110 mV and was again well separated (140 mV) from the third process. Although well-defined, the third and fourth oxidation waves are closely spaced (<100 mV), while separation between the fourth and fifth

dx.doi.org/10.1021/ic401163y | Inorg. Chem. 2013, 52, 9496−9510

oxidation waves is relatively large (120 mV). Overall, the higher rotational barrier for ferrocene substituents in the more sterically crowded FcInTFcP complex results in significantly better resolved redox waves compared to those observed in ClInTFcP and HOInTFcP compounds.

The electrochemical experiments' comproportionation constants (K_c)[24] for all possible mixed-valence states in XInTFcP complexes are presented in Supporting Information, Table S1. Based on electrochemical data, it is expected that the K_c for the first two equatorial ferrocene-groups' oxidation processes, $[MTFcP]^{n}$ + $[MTFcP]^{(n+2)+} \leftrightarrows 2\ [MTFcP]^{(n+1)+}$; where n = 0 for ClInTFcP and HOInTFcP and n = 1 for FcInTFcP, favor stability of mixed-valence species of general formula $[MTFcP]^{n+}$ (n = 1 for ClInTFcP and HOInTFcP and n = 2 for FcInTFcP), which is similar to the other ferrocenyl-containing porphyrins.[6h,m,o] Estimated values of K_c for the second and third oxidation process are significantly smaller (Supporting Information, Table S1), reflecting possible difficulties with generation of spectroscopically pure $[MTFcP]^{n+}$ (n = 2 or 3 for ClInTFcP and HOInTFcP and n = 3 or 4 for FcInTFcP) mixed-valence species. As usual, it should be noted that although estimated values of K_c could be helpful in characterization of the mixed-valence species generated under spectroelectrochemical conditions, they should be treated with a great caution because the electrochemical redox potentials of potentially mixed-valence compounds are highly dependent on a solvent and electrolyte.[6m,24]

To obtain spectroscopic signatures of $[XInTFcP]^{n+}$ species as well as provide an accurate assignment of electrochemically observed redox processes, all XInTFcP complexes were further investigated by the spectroelectrochemical approach. During oxidation under the first oxidation potential, the Soret band of ClInTFcP and HOInTFcP complexes was found to decrease in intensity and undergo a red shift of ~5 nm, while the Q-band was found to decrease in intensity without energy change. In addition, a very characteristic intervalence charge-transfer (IVCT) band appeared at ~950 nm (Figures 7 and Supporting

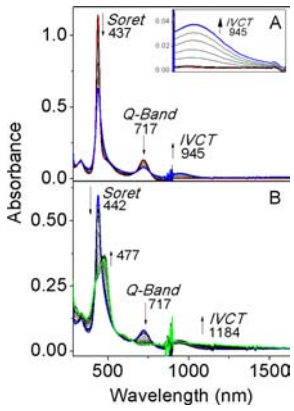

Figure 7. Spectroelectrochemical oxidation of the ClInTFcP complex at first (A) and second (B) oxidation potentials.

Information, Figure S12). The IVCT band energy and intensity are similar to those observed in $[H_2TFcP]^+$ and $[MTFcP]^+$ mixed-valence complexes.[6m,o,q,r] Thus, the first transformation process could be confidently assigned to a XInTFcP → $[XInTFcP]^+$ + e^- (X = Cl^-, OH^-) transformation. Further oxidation of the $[XInTFcP]^+$ (X = Cl^-, OH^-) species under spectroelectrochemical conditions resulted in the Soret band transformation from ~440 nm to ~475 nm, a drop in intensity of the Q-band, and the development of a new broad IVCT band at ~1150−1200 nm. Taking into consideration the small difference between second and third oxidation waves as observed in electrochemical experiments and thus the small values of comproportionation constants, the resulting spectra most likely could be attributed to a mixture of $[XInTFcP]^{2+}$ and $[XInTFcP]^{3+}$ species, which can explain the presence of a very broad NIR IVCT band. Further oxidation of the previously generated mixed-valence species results in gradual disappearance of the entire spectrum, which can be attributed to the decrease in solubility of highly charged $[XInTFcP]^{4+}$ species in low polarity solvent (DCM). Such behavior was observed earlier with H_2TFcP and MTFcP complexes.[6m,o,q,r]

Stepwise oxidation of the ferrocene substituents in the FcInTFcP complex allowed us to differentiate between oxidation of the axial ferrocene group and equatorial porphyrin core ferrocene substituents. Indeed, if the first electron is removed from the equatorial ferrocene group, it should result in a prominent IVCT band in the NIR region, similar to the IVCT band associated with formation of the $[XInTFcP]^+$, $[H_2TFcP]^+$, and $[MTFcP]^+$ mixed-valence complexes.[6m,o,q,r] If, however, the first electron is removed from the axial ferrocene group, then the nature of $[FcTFcP]^+$ species should resemble class I (in Robin−Day classification)[25] compounds and thus no IVCT band should be observed in NIR region. The spectroelectrochemical oxidations of the FcInTFcP complex under the first oxidation potential resulted in an increase in intensity and a small red shift of the Soret band as well as a decrease in intensity and small red shift of the Q-band in the UV−vis spectrum (Figure 8). No IVCT band was observed in the NIR 900−1600 nm region. Because the IVCT band was not developed during this first oxidation process, as well as based on similarity of the resulting spectrum of $[FcInTFcP]^+$ to the

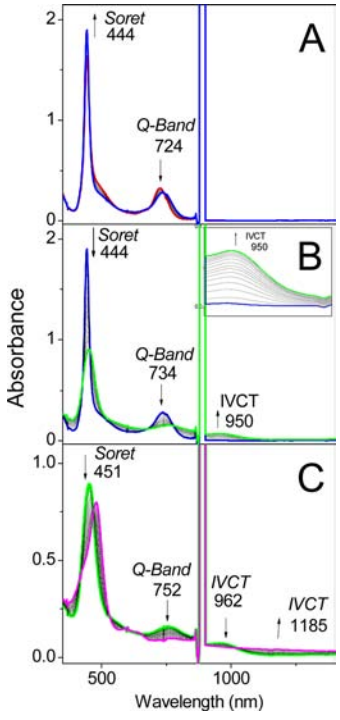

Figure 8. Spectroelectrochemical oxidation of the FcInTFcP complex at first (A), second (B), and third (C) oxidation potentials.

dx.doi.org/10.1021/ic401163y | Inorg. Chem. 2013, 52, 9496−9510

neutral XInTFcP and MTFcP complexes, it could be concluded that the first oxidation is localized at the axial ferrocene group. The next anodic oxidation of $[FcInTFcP]^{+}$ under spectroelectrochemical conditions resulted in a decrease of the Soret band intensity and its red shift as well as a decrease in the Q-band intensity. More importantly, during the second oxidation, formation of a well-defined IVCT band at ~950 nm was clearly observed. This band appeared in approximately the same energy region as that observed for the ClInTFcP and HOInTFcP complexes. Thus, it can be concluded that in the mixed-valence $[FcInTFcP]^{2+}$ complex, one iron(III) center is localized at an axial, and another at an equatorial position. Further oxidation of $[FcInTFcP]^{2+}$ compound results in decrease of the Soret band intensity and its red shift, a further decrease of the Q-band intensity, and the development of a new, broad IVCT band at ~1200 nm, similar to that observed in the likely mixture of $[XInTFcP]^{2+}$ and $[XInTFcP]^{3+}$ (X = Cl^{-} or OH^{-}) species. Again, because of the low solubility of $[FcInTFcP]^{4+/5+}$ species under spectroelectrochemical conditions in our solvent/electrolyte system, we were not able to gain any spectrocopic signatures for those cations.

Overall, spectroelectrochemical experiments allowed us to obtain the spectroscopic signatures of several mixed-valence cations originating from stepwise oxidation of XInTFcP compounds. Spectroelectrochemical experiments suggest that the first electron in FcInTFcP compounds is removed from the axial ferrocene group. Each mixed-valence cation displays characteristic IVCT bands in the NIR region of UV−vis−NIR spectra. Each successful removal of the electron from the mixed-valence complexes results in a low-energy shift of this IVCT band.

Spectroelectrochemical data were further supported by chemical oxidation of XInTFcP complexes. In particular, chemical oxidation of ClInTFcP and HOInTFcP complexes by a controlled amount of silver triflate (AgOTf) or 2, 3-dichloro-5, 6-dicyanobenzoquinone (DDQ) results in transformation of initial XInTFcP compounds into mixed-valence $[XInTFcP]^{+}$ cations (Figures 9 and Supporting Information, Figure S13). During these oxidations, both Soret and Q-bands

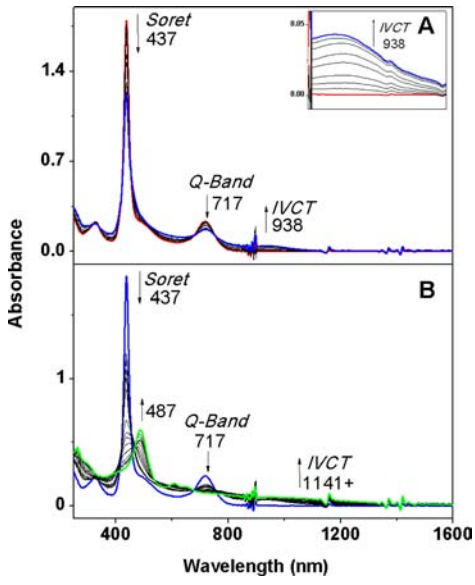

Figure 9. Stepwise chemical oxidation of the ClInTFcP complex by AgOTf in DCM.

decrease in intensity, while a new IVCT band at ~950 nm appears in the UV−vis−NIR spectra of $[XInTFcP]^{+}$ cations. Such transformation is in excellent agreement with the spectroelectrochemical data. Further oxidative titrations of the mixed-valence $[ClInTFcP]^{+}$ compounds result in the rise of a second broad IVCT band at ~1050 nm and a red shift of the Soret band from 437 to 487 nm, again in agreement with the spectroelectrochemical data. Similarly, chemical oxidation of the FcInTFcP complex correlates well with spectroelectrochemical data and results in an intensity increase and blue shift of the initial Soret band and a slight shift of the Q-band at 720 nm. Since no IVCT band is apparent in the UV−vis−NIR spectrum of the $[FcInTFcP]^{+}$ complex, it could be concluded that the first oxidation takes place at the axial ferrocene substituent (Figure 10).

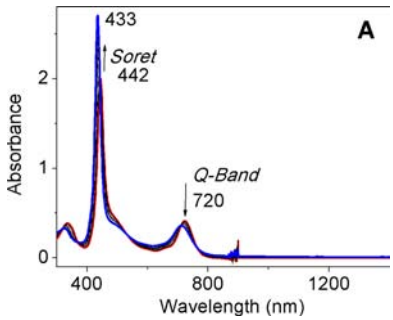

Figure 10. Oxidation of the FcInTFcP complex to $[FcInTFcP]^{+}$ by AgOTf in DCM.

The Hush method[26] is typically used for the initial analysis of experimental data in mixed-valence compounds. In the case of XInTFcP compounds, such analysis could be applied to the spectroelectrochemically or chemically generated mixed-valence $[ClInTFcP]^{+}$, $[HOInTFcP]^{+}$, and $[FcInTFcP]^{2+}$ species because of the presence of a well-defined IVCT band in the NIR region of their UV−vis−NIR spectra. The two key parameters that are estimated using the Hush model are the electronic coupling matrix element (H_{ab}) and the degree of delocalization (α^2). Supporting Information,Table 2 displays the parameters obtained from the IVCT band fits (Supporting Information, Figure S14), which are only estimates that add support to the other spectroscopic data discussed above. In all cases, the H_{ab} and α values closely match the values obtained for the previously reported polyferrocenyl porphyrins,[6m,o,q,r] and are in the range of Class II (Robin and Day classification) mixed-valence compounds.[27]

Electronic Structures and Atropisomerism in XInTFcP Complexes. DFT calculations were performed to acquire insight into the nature of the electronic structure, spectroscopy, and redox properties of XInTFcP complexes. Because of the great similarities in properties of ClInTFcP and HOInTFcP compounds, the electronic structures and energies of individual atropisomers of only ClInTFcP and FcInTFcP complexes were compared. Moreover, because of the large similarities between electronic structures of individual atropisomers, only the detailed analysis of electronic structures of ClInTFcP and FcInTFcP determined by the X-ray geometries will be discussed below.

The molecular orbital energy diagram, molecular orbital compositions, and representative shapes of important molecular orbitals predicted using the BP86 exchange-correlation func-

dx.doi.org/10.1021/ic401163y | Inorg. Chem. 2013, 52, 9496−9510

tional and DGDZVP (In) /6-311G(d) (all other atoms) basis sets are shown in Figure 11 and Supporting Information, Figure

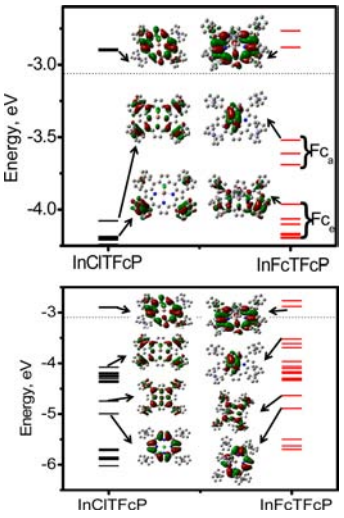

Figure 11. Molecular orbital diagram of ClInTFcP and FcInTFcP complexes calculated with X-ray geometries and BP86 exchange-correlation functional. The HOMO−LUMO area is presented on a top.

S15. Electronic structures of the ClInTFcP and FcInTFcP complexes have many similarities. In particular, (i) the lowest unoccupied molecular orbital (LUMO) and LUMO+1 are predominantly porphyrin-centered π^* orbitals, that resemble Gouterman's[28] classic e_g symmetry MO pair; (ii) similar to all previously described MTFcP and H_2TFcP compounds, predominantly ferrocene-containing MOs have higher energies compared to the occupied porphyrin-centered π-orbitals; (iii) the highest MO with predominant equatorial ferrocene group character (MO 301 for ClInTFcP and MO 337 for FcInTFcP, Supporting Information, Figure S15) have ∼10% of their contribution from the porphyrin π-system mostly located at *meso*-carbon and nitrogen atoms; (iv) the "a_{2u}"-type (with most electron density located at the *meso*-carbon and nitrogen atoms) porphyrin-centered π-orbitals (MO 289 for ClInTFcP and MO 325 for FcInTFcP) has a higher energy than the "a_{1u}"-type (with most electron density located at the pyrrolic α- and β-carbon atoms) porphyrin-centered π-orbital (MO 288 for ClInTFcP and MO 324 for FcInTFcP); (v) all 12 predominantly equatorial ferrocene group centered MOs are spaced closely together (∼0.4 eV) and are well-separated (∼0.5 eV) from the porphyrin-centered π-orbitals. Such electronic structure similarities dictate that the oxidation of the ferrocene substituents in ClTFcP and FcTFcP complexes should happen prior to oxidation of the porphyrin π-system. In the case of the FcInTFcP complex, DFT calculations predict that the highest occupied molecular orbital (HOMO) to HOMO-2 are almost exclusively centered at the axial ferrocene ligand and these three MOs are energetically separated from the remaining 12 equatorial ferrocene-centered MOs. Thus, in agreement with electrochemical, spectroelectrochemical, and chemical oxidation data, DFT calculations predict that the first oxidation in the FcInTFcP complex should be centered at the axial ferrocene ligand.

So far, out of the five reported X-ray structures of MTFcP compounds, two (H_2TFcP and ZnTFcP)[6m,7d] crystallize as $\alpha,\beta,\alpha,\beta$-, two ($Cl_2$SnTFcP and ClInTFcP)[6r] as $\alpha,\alpha,\beta,\beta$-, and one (FcInTFcP) as $\alpha,\alpha,\alpha,\alpha$-atropisomers. The simplest explanation for such observed atropisomerism is that crystal packing forces can easily overcome a small rotational barrier for ferrocene substituents. Such a hypothesis is supported by the variable-temperature NMR experiments. To explore energetics of atropisomers of XInTFcP complexes and gain a better understanding of discrepancies in X-ray crystal structures of MTFcP compounds, we conducted an array of the geometry optimizations for all possible atropisomers of ClInTFcP and FcInTFcP. Taking into account that GGA-type exchange-correlation functionals are usually not recommended for calculation of the energy profiles for isomerism cases,[29] a hybrid (25% of Hartree−Fock exchange) PBE1PBE exchange-correlation functional was used along with an ECP LANL2DZ basis set (see Experimental Section for detailed discussion on the choice of computational method).

The energy profiles for individual atropisomers of the ClInTFcP and FcInTFcP complexes are presented in Figure 12. Similar to previous studies on MTFcP complexes,[6l,m,o] in

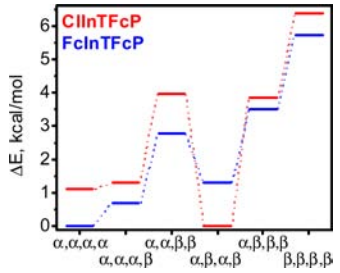

Figure 12. DFT predicted energy profiles for atropisomers of ClInTFcP (red) and FcInTFcP (blue) complexes.

the case of the ClInTFcP complex, the lowest energy DFT-predicted atropisomer is $\alpha,\beta,\alpha,\beta$, while $\alpha,\alpha,\alpha,\alpha$ and $\alpha,\alpha,\alpha,\beta$ atropisomers have only 1.1 and 1.3 kcal/mol higher energy, respectively. On the other hand, DFT predicted that the crystallographically observed $\alpha,\alpha,\beta,\beta$-atropisomer should have 3.9 kcal/mol higher energy compared to the most stable $\alpha,\beta,\alpha,\beta$-atropisomer. Finally, the β,β,β,β-atropisomer was predicted to have the highest energy out of all possible ferrocene group arrangements. In the case of the FcInTFcP complex, DFT calculations predict that the crystallographically observed $\alpha,\alpha,\alpha,\alpha$-atropisomer indeed should have the lowest energy. However, $\alpha,\alpha,\alpha,\beta$- and $\alpha,\beta,\alpha,\beta$-atropisomers are only 0.7 and 1.3 kcal/mol higher in energy than the most stable $\alpha,\alpha,\alpha,\alpha$-atropisomer. Again, the β,β,β,β-atropisomer has the highest energy. It should be noted, however, that in both studied XInTFcP complexes, the energy difference between the most stable and the least stable atropisomers was found to be about 6 kcal/mol, which correlates very well with the hypothesis mentioned above where crystal packing forces are able to overcome the rotational barrier for ferrocene group rotation in MTFcP compounds.

Noncovalent Complex Formation between FcInTFcP and C_{60} Fullerene. Since ferrocene-containing porphyrins with organometallic groups directly linked to the porphyrin core are shown to be effective dyads for photoinduced electron transfer processes,[11,12] it was tempting to see whether or not such donor-antennae dyads could be cocrystallized with the typical electron-acceptor, C_{60} fullerene. Such donor-antennae-acceptor noncovalent assemblies could form photoinduced long-lived Fc^+-MTFcP-$C_{60}^{-\cdot}$ charge-separated states potentially

dx.doi.org/10.1021/ic401163y | Inorg. Chem. 2013, 52, 9496−9510

useful for application in OPVs. Upon slow evaporation of a solution of FcInTFcP and C_{60}, we observed formation of large (up to several mm!) dark-colored monocrystals, which were analyzed by X-ray diffraction. Refinement parameters for the FcInTFcP@4C_{60} noncovalent assembly are presented in Table 1 while selected bonds lengths and angles are summarized in Table 2. ORTEP diagrams of FcInTFcP@4C_{60} are shown in Figures 13 and 14.

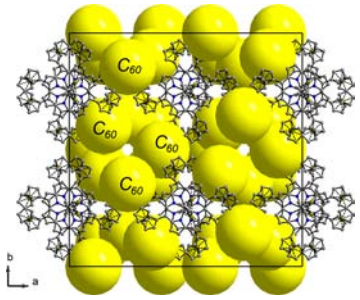

Figure 13. Perspective view of the FcInTFcP@4C_{60} assembly along the crystallographic *c*-axis. C_{60} molecules are represented by spheres for clarity.

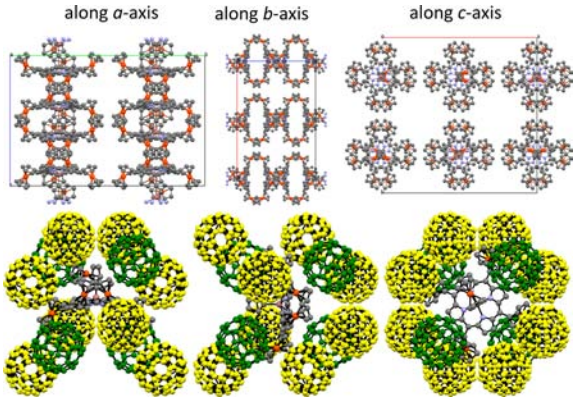

Figure 14. Perspective view of the FcInTFcP@4C_{60} assembly along crystallographic axes. In the top figures, all C_{60} molecules are omitted for clarity. The bottom figures show how individual FcInTFcP complexes interact with two types of C_{60} molecules in the unit cell. Two independent C_{60} molecules are color coded in green and yellow.

The FcInTFcP complex adopts an *α,β,α,β*-conformation with the indium ion located 0.912 Å above the porphyrin N4 plane. The In−C(Fc) bond distance in FcInTFcP@4C_{60} (2.205(13) Å) was found to be longer compared to the In−C(Fc) bond distance in the standalone FcInTFcP complex (2.152 Å). Similarly, the average In−N bond distance in the FcInTFcP@C_{60} assembly (2.231(5) Å) is longer compared to that in the standalone FcInTFcP (2.201 Å). The observed *α,β,α,β*-conformation of FcInTFcP in FcInTFcP@4C_{60} and the *α,α,α,α*-conformation in the standalone FcInTFcP again confirm the small energy differences between possible FcInTFcP atropisomers as determined by DFT calculations.

Each FcInTFcP molecule crystallizes with C_{60} fullerene molecules in a 1:4 ratio, and all our attempts to cocrystallize FcInTFcP with C_{60} with different ratios failed. FcInTFcP molecules in the FcInTFcP@4C_{60} assembly form infinite chains along a crystallographic *c*-axis, separated by C_{60} fullerene channels. The equatorial ferrocene substituents from different FcInTFcP chains are closely spaced (the closest Fc(C)-Fc(C) intermolecular contact was found at 3.528 Å and the closest Fc(H)-Fc(H) contact was found at 3.157 Å). Intermolecular interactions between the axial and the equatorial ferrocene ligands or the axial ferrocene ligand and the neighboring porphyrin core within the same FcInTFcP column are much weaker. The closest Fc_{ax}(C)-Fc_{eq}(C) contact was found at 4.644 Å, while the axial ferrocene ligand is located at ∼7 Å from the neighboring porphyrin plane. The skew angle N(A)-In(A)-In(B)-N(B) for the neighboring FcInTFcP molecules in the same column was found to be 42.05°.

The remarkable feature of the FcInTFcP@4C_{60} structure is the formation of C−H---*π* and C---*π* interactions only between Cp rings of the ferrocenyl groups and fullerene molecules.[30] In contrast to numerous numbers of structures of porphyrin-C_{60} adducts reported in CSD no *π*---*π* interactions were observed between the aromatic systems of the porphyrin core and the fullerenes. Both ferrocenyl groups form two types of contacts by means of C−H---*π* and *π*---*π* interactions. The axial ferrocenyl group is surrounded by four fullerene molecules (Figure 14a), while equatorial ferrocenes are surrounded by five fullerene groups (Figure 14b). Only the unsubstituted Cp ring of the axial ferrocenyl group is involved in the formation of the weak interactions. Thus C(Cp)---C(C60) distance is 3.28 Å, while C−H(Cp)---C(C60) distance is 2.57 Å. Contacts formed via substituted Cp ring C−H(Cp)---*π*(C60) are longer and equal to 2.96 Å. No *π*(Cp)---*π*(C60) interactions were observed for the substituted Cp ring of the axial ferrocenyl group. That can be attributed to fullerene-fullerene and fullerene-porphyrin interactions which determine the size of the cage where the axial ferrocene is located. The C_{60}(center)---C_{60}(center) distances were estimated to be 9.874 Å for equivalent C_{60} molecules and 10.143−10.523 Å for non-equivalent C_{60} molecules. The first distance is slightly shorter and the second distance is slightly longer than the C_{60} van der Waals diameter (10.18 Å). The equatorial ferrocenes are less shielded by the porphyrin core and thus both Cp rings form C(Cp)--C(C60) contacts with fullerene molecules. These contacts are within the range 3.12 Å−3.37 Å. Also, equatorial ferrocenes form more C−H(Cp)---*π*(C60) contacts. They range from 2.48 Å to 2.98 Å.

Overall, the FcInTFcP@4C_{60} structure represents an excellent motif for the light-harvesting module in OPVs. Indeed, there are two highly directional channels that could be clearly seen in the structure: (i) a light-harvesting channel, which consists of porphyrin chain oriented along crystallographic *c*-axis; (ii) electron-transfer C_{60} spiral channels oriented along the same crystallographic axis. Thus, it is possible to expect that electron-transfer from the ferrocene donor to the photoexcited porphyrin antennae would facilitate electron injection to the fullerene channels. Once at the highly anisotropic fullerene channel, an electron could preferentially travel along the channel to the conducting electrode completing the photocurrent cycle.

In general, porphyrin-fullerene noncovalent supramolecular assemblies can significantly differ in their electronic structure, and can span over three major classes:[12] (i) neutral porphyrin−neutral C_{60} fullerene existing as weakly interacting cocrystallization products; (ii) charge transfer (porphyrin to C_{60} fullerene) complexes; (iii) radical ion salts in which porphyrin is oxidized and C_{60} fullerene is reduced. To get insight into the nature of FcInTFcP: C_{60} fullerene interactions, we conducted DFT calculations on optimized structures of FcInTFcP and C_{60} molecules as well as recorded UV−vis spectra of mixtures of

dx.doi.org/10.1021/ic401163y | Inorg. Chem. 2013, 52, 9496−9510

these compounds in solution. A molecular orbital diagram for the FcInTFcP and C_{60} molecules is presented in Figure 15.

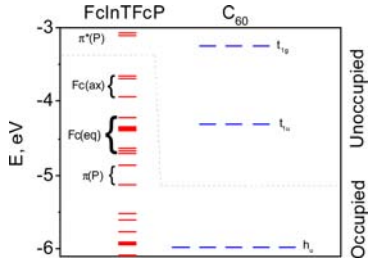

Figure 15. DFT predicted energies of frontier MOs of the FcInTFcP and C_{60}.

DFT calculations suggest that the HOMO to HOMO-3 MOs of the FcInTFcP complex have 0.09−0.66 eV higher energies than the triply degenerate LUMO to LUMO+2 t_{1u} MOs of C_{60} fullerene. The HOMO to HOMO-3 MOs of the FcInTFcP complex are predominantly localized on axial (HOMO to HOMO-2) and equatorial (HOMO-3) ferrocene ligands thus allowing potential charge-transfer to the LUMO of C_{60}. The energies of LUMO and LUMO+1 in the FcInTFcP complex are ~0.15 eV higher than the energy of the triply degenerate t_{1g} set in C_{60}. Thus, population of predominantly porphyrin-centered LUMO and LUMO+1 of the FcInTFcP complex upon photoexcitation can potentially result in further electron transfer from these MOs to unoccupied t_{1g} or t_{1u} sets of C_{60}, which could potentially result in formation of long-lived charge-separated Fc-InTFcP^{+}-C_{60}^{-}. and Fc^{+}-InTFcP-$C_{60}^{-\cdot}$ states.

To provide an experimental estimation of the degree of interaction of FcInTFcP and C_{60}, UV−vis−NIR spectra for the incremental titration of the FcInTFcP complex with C_{60} were recorded (Supporting Information, Figure S16). The following results were obtained during titration experiments: (i) all spectra essentially represent a superposition of the absorption spectra of FcInTFcP and C_{60}; (ii) Soret band intensity increases by ~3% and Q-band intensity decreases by ~3% during the 0−100 equivalents titration; (iii) difference spectra analysis in the NIR region suggest small decreases in the Q-band and appearance of a new weak band at ~750 nm along with appearance of several weak bands between 900 and 1100 nm. Although these bands can be attributed to charge-transfer bands between FcInTFcP and C_{60},[12] they also could arise because of oxidation of a small fraction of FcInTFcP in solution. Thus, UV−vis−NIR titration experiments indicate a weak if any interaction of FcInTFcP with C_{60} fullerene and probably suggest that in the FcInTFcP@4C_{60} assembly, porphyrin and C_{60} molecules could be viewed as essentially neutral, weakly interacting fragments.

CONCLUSIONS

Three new indium(III) metalated poly(ferrocenyl)-containing porphyrins have been prepared and characterized by a variety of spectroscopic methods. Structures of ClInTFcP, FcInTFcP, and FcInTFcP@4C_{60} compounds have been reported. To the best of our knowledge, the last structure represents the first example of a cocrystallized organometallic porphyrin and C_{60} fullerene. The redox properties of all new compounds were also examined by electrochemical methods, while the nature of mixed-valence species of general formula $[XInTFcP]^{n+}$ was probed by spectroelectrochemical and chemical oxidation approaches. It was found that the In−C σ-bonded ferrocene substituent has lower oxidation potentials compared to the equatorial organometallic groups. The electronic structure, energy profiles of all possible atropisomers, and the interaction of FcInTFcP with C_{60} were probed by DFT calculations. It was suggested that in the FcInTFcP@4C_{60} assembly, porphyrin and C_{60} molecules could be described as essentially neutral, weakly interacting fragments.

EXPERIMENTAL SECTION

Materials. All reactions were performed under a dry argon atmosphere with flame-dried glassware. All solvents and reagents were purchased from commercial sources and used without additional purification. Dry toluene was obtained by distillation over sodium, dry DCM was obtained by distillation over calcium hydride prior to experiments, and dry THF was obtained by distillation over Na/K alloy with benzophenone. Silica gel (60 Å, 63−100 μm) needed for column chromatography was purchased from Dynamic Adsorbents, while basic aluminum oxide (Activity I, 58 Å, 150 mesh) was purchased from Fischer Inc. The tetrabutylammonium tetrakis-(pentafluorophenyl)borate (TBAF) was used in anhydrous DCM for electrochemical studies, after preparation according to literature procedures.[23]

Instrumentation. A Varian Unity INOVA NMR instrument was used to obtain spectra at 500 MHz frequency for protons and 125 MHz for carbons. Each spectrum was referenced to TMS as an internal standard, and chemical shifts were recorded in parts per million. All UV−vis data was obtained on a JASCO-720 spectrophotometer at room temperature. An OLIS DCM 17 CD spectropolarimeter with 1.4 T DeSa magnet was used to obtain all MCD data. Electrochemical measurements were conducted using a CHI-620C electrochemical analyzer utilizing the three-electrode scheme. Either carbon or platinum working, auxiliary and reference electrodes were used in 0.05 M solution of TBAF in DCM with redox potentials corrected using an internal standard (decamethylferrocene) in all cases. Spectroelectrochemical data were collected using a custom-made 1 mm cell, a working electrode made of platinum mesh, and a 0.15 M solution of TBAF in DCM. Elemental analyses were performed by Atlantic Microlab, Inc. in Atlanta, Georgia.

Syntheses. *Synthesis of ClInTFcP.* LiN[Si(CH$_3$)$_3$]$_2$ (1.6 g; 9.0 mmol) was added to a solution of metal-free 5,10,15,20-tetraferrocenylporphyrin[6m] (800 mg; 0.766 mmol) in 160 mL of dry THF, and the reaction was allowed to continue for 15 min. After this period of time, $InCl_3$ (4.0 g; 18.0 mmol) was added and the reaction mixture was refluxed for 3 h (controlled by UV−vis). The reaction mixture was cooled down, the solvent was evaporated to dryness under vacuum, and the resulting solid residue was purified by column chromatography on silica gel using DCM, ethyl acetate, THF, and ethanol as eluents. The main fraction (ClInTFcP) was collected, and the solvent was removed under reduced pressure. The residue was washed several times with hexanes and dried in vacuum. Yield: 475 mg (52%). ^{1}H NMR (500 MHz, $CDCl_3$, TMS), δ (ppm) = 4.25 (s, 20H, Cp), 4.86 (s, 8H, β-Cp), 5.54 (s, 8H, α-Cp), 10.02 (s, 8H, β-Pyrrole). ^{13}C NMR (125 MHz, $CDCl_3$, TMS), δ (ppm) = 69.29 (β-Cp), 70.63 (Cp), 76.02 (α-Cp), 89.99 (C_{ipso}), 120.30 (C_{meso}), 131.62 (β-Pyrrole), 149.28 (α-Pyrrole). Anal. Calc. for ClInTFcP × H_2O (found): C 59.43 (58.79), H 3.82 (3.77), N 4.62 (4.85). MS (APCI, THF, m/z): 1194 $[M]^+$ 1231 $[M\text{-}Cl\text{+}THF]^+$

Synthesis of HOInTFcP. A solution of ClInTFcP (30 mg; 0.025 mmol) in 30 mL of DCM was shaken with an aqueous solution of sodium hydroxide (2M) (3 × 10 mL), water (3 × 10 mL) and dried over anhydrous sodium sulfate. DCM was removed under reduced pressure, and the product was recrystallized from DCM/Hexane mixture and dried in air. Yield: 4 mg (14%). ^{1}H NMR (500 MHz, $CDCl_3$, TMS), δ (ppm) = −5.37 (s, br, 1H, OH), 4.36 (s, 20H, Cp), 4.86 (s, 8H, β-Cp), 5.54 (s, 8H, α-Cp), 10.02 (s, 8H, β-Pyrrole). ^{13}C NMR (125 MHz, $CDCl_3$, TMS), δ (ppm) = 69.05 (β-Cp), 71.01 (Cp), 78.09 (α-Cp), 90.71 (C_{ipso}), 120.02 (C_{meso}), 131.13 (β-

dx.doi.org/10.1021/ic401163y | Inorg. Chem. 2013, 52, 9496−9510

Pyrrole), 150.03 (α-Pyrrole). Anal. Calc. for HOInTFcP (found): C 61.27 (61.48), H 3.86 (4.00), N 4.76 (4.55).

Synthesis of FcInTFcP. To a solution of ferrocene iodide (196.2 mg; 0.629 mmol) in 8 mL of dry ether a butyl lithium solution in hexane (0.26 mL; 2.5M) was added dropwise at −78 °C (CO_2/acetone) with continuous stirring. After stirring for 5 min in the low temperature cold bath, the mixture was warmed to room temperature to complete the reaction. Ferrocenyl lithium salt was added via syringe to a solution of InClTFcP (145 mg; 0.121 mmol) in 10 mL of dry toluene at room temperature. The reaction mixture was stirred for 45 min at room temperature before being quenched with 8 mL of distilled water. All solvents were removed under vacuum, and the solid residue was purified by column chromatography using toluene as eluent. Yield: 94 mg (58%). ^{1}H NMR (500 MHz, THF-d_8, TMS), δ (ppm) = 0.85 (s, 2H, α-Cp_{ax} In coordinated Fc), 2.55 (s, 5H, Cp_{ax} In coordinated Fc), 2.95 (s, 2H, β-Cp_{ax} In coordinated Fc), 4.26 (s, 20H, Cp_{eq} porphyrin Fc), 4.93 (s, 8H, β-Cp_{eq} porphyrin Fc), 5.52 (s,8H, α-Cp_{eq} coordinated Fc), 9.91 (s, 8H, β-Pyrrole). ^{13}C NMR (125 MHz, THF-d8, TMS), δ (ppm) = 66.65 (Cp_{ax} In coordinated Fc), 67.87 (β-Cp_{ax} In coordinated Fc), 69.16 (β-Cp_{eq} porphyrin Fc), 70.85 (Cp_{eq} porphyrin Fc), 71.06 (α-Cp_{ax} In coordinated Fc), 72.52 (α-Cp_{eq} porphyrin Fc), 90.36 (Cp_{ipso}, porphyrin Fc), 119.36 (C_{meso}), 132.14 (β-Pyrrole), 149.31 (α-Pyrrole). Anal. Calc. for FcInTFcP (found): C 62.69 (62.63), H 4.22 (4.25), N 4.12 (3.98). MS (APCI, THF, m/z): 1345 $[M]^+$

Computational Aspects. All computations were performed using Gaussian 09 software running under Windows or UNIX OS.[31] MO contributions were compiled from single point calculations using the VMOdes program.[32] In all single-point calculations, Becke's exchange functional and the Pedrew 86 correlation functional (BP86)[33] were used because as it was shown before, they provide a good electronic structure description for ferrocene-containing molecules,[34] including ferrocenylporphyrins.[6p,o,34a] Use of hybrid B3LYP[35] or PBE1PBE[36] exchange-correlation functionals lead to heavy infusion of porphyrin-centered π-electron density into the HOMO region, which was not supported by the experimental data. Wachter's full-electron basis set was used for iron,[37] DGauss DZDVP basis set was used for the indium ion,[38] while for all other atoms the 6-311G(d) basis set[39] was employed. In all atropisomers energy profile calculations, the PBE1PBE exchange-correlation functional was used. Our test calculations indicate that use of this correlation functional results in slightly better agreement in calculated bond distances and angles compared to BP86 and B3LYP functionals. Taking into consideration the size of the target molecules, the ECP LANL2DZ basis set[40] was used for all atoms in all atropisomer calculations. Each atropisomer under consideration was calculated using several possible local starting geometries to ensure that the smallest energy per atropisomer was achieved. The C_{60} molecule was optimized in the I_h point group using the PBE1PBE exchange-correlation functional and the LANL2DZ basis set, while in single-point calculations the 6-311G(d) basis set was used to match energy profile of FcInTFcP.

X-ray Crystallography. X-ray quality single crystals of the ClInTFcP and FcInTFcP complexes were grown from slow diffusion of their saturated toluene solutions with pentane. Single crystals of FcInTFcP@4C_{60} were grown by slow evaporation of saturated toluene solution. Experimental data for all compounds were collected using a Rigaku Rapid II X-ray diffractometer with curved IPDS detector using graphite-monochromatized Mo-$K\alpha$ radiation (λ = 0.71075 Å).

The structures of the ClInTFcP and FcInTFcP compounds were solved by the direct method using the SIR-92 program.[41] All missed non hydrogen atoms were located from analysis of a difference Fourier-map and refined isotropically, followed by anisotropic approximations. All aromatic hydrogen atoms were placed geometrically while hydrogens for the methyl group of toluene solvent molecules were located from the difference Fourier-map analysis and were constrained. Thermal displacement parameters for hydrogen atoms were constrained to the parent atom with $U_{iso}(H) = 1.2U_{eq}(C)$ for methylene and aromatic hydrogens including those on the porphyrin system, while $U_{iso}(H) = 1.5U_{eq}(C)$ for the methyl group of the solvent, so-called "riding mode" ($U_{eq} = 1/3(U_{11} + U_{22} + U_{33})$). The structures were completely refined using full-matrix least-squares methods and the SHELXL-97 program.[42]

The indium-chloride moiety in the ClInTFcP complex was found to be statically disordered over two positions. Indeed, such disorder is very common for indium containing macrocycles and is induced by the five-coordinate central ion where the metal atom lies out of porphyrin plane. Final refined populations for the two positions were 0.84 and 0.16, respectively. In the crystal structure, the position of the minor component of the indium-chloride moiety (In1b-Cl1b) overlaps with the position of the toluene molecule (C61−C67). For this reason, the population of the toluene molecule position is less than one and related to the In−Cl part. The two positions were refined together with like related variables and with a total contribution to the population equal to 1. The best value for R_1 was 0.051, but the difference electron density map analysis revealed five peaks, 3.35, 3.03 2.23, 2.08, 2.05 $e^-/Å^3$, that correspond to a disordered pentane molecule (a toluene/pentane solvent system was used for crystallization of ClInTFcP). It is a well-known fact that it is very difficult to correctly model disorder of alkane chains. Unfortunately, such disorder could not be resolved, so the SQUEEZE procedure implemented in the PLATON[43] program was used to remove a contribution from the disordered area. Afterward, refinement was successfully completed with a final R_1 equal to 0.039 and a maximum/minimum of electron density equal to 0.6/−0.45 $e^-/Å^3$. MERCURY[44] and PLATON/PLUTON[43] software were used for visualizing the results. The structure FcInTFcP@4C_{60} was solved by the direct method implemented in the SHELXS-97[42] program and refined using the SHELXL-2013 program.[42] The compound crystallizes in a tetragonal symmetry, $I4_1/acd$ space group (origin at −1). The porphyrin system and equatorial ferrocenyl groups adopt −4 symmetry while the indium metal and the axial ferrocene group are disordered over symmetry elements (−4 axis). The indium metal and the ipso carbon atom of the axial ferrocenyl group lie on a special position (0.5, 0.25, z) and are disordered over two positions. The occupation factors were constrained to be 0.5 for both atoms. All other atoms of the axial ferrocenyl group are disordered over four positions by a −4 symmetry operation and thus occupation factors were constrained to be 0.25. One C_{60} molecule is also disordered over the symmetry element (2-fold axis) and thus all occupation factors were constrained to be 0.5. The second C_{60} molecule was found to be disordered over two positions. The occupation parameters for both parts were refined, while their sum was constrained to be 1. After refinement the occupation factors from both parts are 0.47 and 0.53. A number of 1,2 and 1,3 bond restraints were applied for the fullerene molecules and the axial ferrocenyl group (DFIX, DANG, SADI). All atoms except hydrogens were refined in an anisotropic approximation and numerous numbers of atom displacement parameters (ADP) restraints were used (DELU, SIMU, and ISOR). The total number of restraints was 760, and the total number of parameters to refine was 1292, while the number of unique reflections was 8438. The structure was refined using full-matrix-block least-squares methods where coordinates and ADPs of each disordered fullerene molecule were refined in individual blocks. The coordinates and ADPs of the FcInTFcP molecule were refined in an individual block as well as together with the fullerene molecules to keep an overlap between the blocks. The overall scale factor was refined in each block. Hydrogen atoms were added geometrically and refined in the "riding" approximation. A weight function has not been refined and was used as proposed by the program $w = 1/[\sigma^2(F_o^2) + (3/5(F_o^2 + 2F_c^2))^2]$, where F_o^2 and F_c^2 are observed and calculated structure amplitudes. All information about the refinement of crystal structures is presented in Tables 1 and 2 above; the corresponding CIF files are presented in the Supporting Information.

■ ASSOCIATED CONTENT

Ⓢ Supporting Information

CIF files for ClInTFcP, FcInTFcP, and FcInTFcP@4C_{60} complexes. DFT optimized coordinates for individual atropisomers of ClInTFcP and FcInTFcP. NMR spectra of

dx.doi.org/10.1021/ic401163y | Inorg. Chem. 2013, 52, 9496−9510

XInTFcP complexes. DPV and IVCT data analysis. This material is available free of charge via the Internet at http://pubs.acs.org.

AUTHOR INFORMATION

Corresponding Author

*E-mail vnemykin@d.umn.edu.

Notes

The authors declare no competing financial interest.

ACKNOWLEDGMENTS

Generous support from the NSF Grant CHE-1110455 and NSF Grant MRI CHE-0922366, Minnesota Supercomputing Institute, and University of Minnesota Grant-in-Aid to V.N., and University of Minnesota UROP Grant to J.R.S. are greatly appreciated. We also wish to acknowledge Dr. Semen Dudkin for help with some titration experiments.

REFERENCES

(1) (a) Wu, Y.; Zhu, W. *Chem. Soc. Rev.* **2013**, *42*, 2039−2058. (b) Balasingam, S. K.; Lee, M.; Kang, M. G.; Jun, Y. *Chem. Commun.* **2013**, *49*, 1471−1487. (c) Li, L.-L.; Diau, E. W.-G. *Chem. Soc. Rev.* **2013**, *42*, 291−304. (d) Gratzel, M. *Acc. Chem. Res.* **2009**, *42*, 1788−1798. (e) Garcia-Iglesias, M.; Cid, J.-J.; Yum, J.-H.; Forneli, A.; Vazquez, P.; Nazeeruddin, M. K.; Palomares, E.; Gratzel, M.; Torres, T. *Energy Environ. Sci.* **2011**, *4*, 189−194. (f) Hagfeldt, A.; Gratzel, M.; Nogueria, A. F.; Furtado, L. F. O.; Formiga, A. L. B.; Nakamura, M.; Araki, K.; Toma, H. E.; Panigrahi, S.; Pal, T. *Chemtracts* **2004**, *17*, 175−182. (g) Chen, X.; Li, C.; Graetzel, M.; Kostecki, R.; Mao, S. S. *Chem. Soc. Rev.* **2012**, *41*, 7909−7937. (h) Nazeeruddin, M. K.; Baranoff, E.; Graetzel, M. *Sol. Energy* **2011**, *85*, 1172−1178. (i) Lee, M. M.; Teuscher, J.; Miyasaka, T.; Murakami, T. N.; Snaith, H. J. *Science* **2012**, *338*, 643−647. (j) Crabtree, R. H. *Organometallics* **2011**, *30*, 17−19. (k) Jacko, A. C.; McKenzie, R. H.; Powell, B. J. *J. Mater. Chem.* **2010**, *20*, 10301−10307. (l) Wong, W.-Y.; Ho, C.-L. *Acc. Chem. Res.* **2010**, *43*, 1246−1256.

(2) (a) Kaim, W.; Sarkar, B. *Coord. Chem. Rev.* **2007**, *251*, 584−594. (b) Fabre, B. *Acc. Chem. Res.* **2010**, *43*, 1509−1578. (c) *Ferrocenes: Ligands, Materials and Biomolecules*; Stepnicka, P., Ed.; John Wiley & Sons, Ltd.: Chichester, England, 2008; p 655.

(3) (a) Nemykin, V. N.; Kobayashi, N. *Chem. Commun.* **2001**, 165−166. (b) Lukyanets, E. A.; Nemykin, V. N. *J. Porphyrins Phthalocyanines* **2010**, *14*, 1−40.

(4) (a) Jin, Z.; Nolan, K.; McArthur, C. R.; Lever, A. B. P.; Leznoff, C. C. *J. Organomet. Chem.* **1994**, *468*, 205−212. (b) Poon, K.-W.; Yan, Y.; Li, X. Y.; Ng, D. K. P. *Organometallics* **1999**, *18*, 3528−3533. (c) Nemykin, V. N.; Lukyanets, E. A. *ARKIVOC* **2010**, *(i)*, 136−208. (d) An, M.; Kim, S.; Hong, J.-D. *Bull. Korean Chem. Soc.* **2010**, *31*, 3272−3278. (e) Gonzalez-Cabello, A.; Claessens, C. G.; Martin-Fuch, G.; Ledoux-Rack, I.; Vazquez, P.; Zyss, J.; Agullo-Lopez, F.; Torres, T. *Synth. Met.* **2003**, *137*, 1487−1488. (f) Gonzalez-Cabello, A.; Vazquez, P.; Torres, T. *J. Organomet. Chem.* **2001**, *637*−*639*, 751−756.

(5) (a) Gryko, D. T.; Piechowska, J.; Jaworski, J. S.; Galezowski, M.; Tasior, M.; Cembor, M.; Butenschoen, H. *New J. Chem.* **2007**, *31*, 1613−1619. (b) Kumar, R.; Misra, R.; PrabhuRaja, V.; Chandrashekar, T. K. *Chem.—Eur. J.* **2005**, *11*, 5695−5707. (c) Venkatraman, S.; Kumar, R.; Sankar, J.; Chandrashekar, T. K.; Sendhil, K.; Vijayan, C.; Kelling, A.; Senge, M. O. *Chem.—Eur. J.* **2004**, *10*, 1423−1432.

(6) (a) Bucher, C.; Devillers, C. H.; Moutet, J.-C.; Royal, G.; Saint-Aman, E. *Coord. Chem. Rev.* **2009**, *253*, 21−36. (b) Loim, N. M.; Abramova, N. V.; Sokolov, V. I. *Mendeleev Commun.* **1996**, 46−47. (c) Burrell, A. K.; Campbell, W. M.; Jameson, G. B.; Officer, D. L.; Boyd, P. D. W.; Zhao, Z.; Cocks, P. A.; Gordon, K. C. *Chem. Commun.* **1999**, 637−638. (d) Narayanan, S. J.; Venkatraman, S.; Dey, S. R.; Sridevi, B.; Anand, V. R. G.; Chandrashekar, T. K. *Synlett* **2000**, 1834−1836. (e) Rhee, S. W.; Na, Y. H.; Do, Y.; Kim, J. *Inorg. Chim. Acta* **2000**, *309*, 49−56. (f) Shoji, O.; Okada, S.; Satake, A.; Kobuke, Y. *J. Am. Chem. Soc.* **2005**, *127*, 2201−2210. (g) Shoji, O.; Tanaka, H.; Kawai, T.; Kobuke, Y. *J. Am. Chem. Soc.* **2005**, *127*, 8598−8599. (h) Auger, A.; Swarts, J. C. *Organometallics* **2007**, *26*, 102−109. (i) Kubo, M.; Mori, Y.; Otani, M.; Murakami, M.; Ishibashi, Y.; Yasuda, M.; Hosomizu, K.; Miyasaka, H.; Imahori, H.; Nakashima, S. *J. Phys. Chem. A* **2007**, *111*, 5136−5143. (j) Nemykin, V. N.; Barrett, C. D.; Hadt, R. G.; Subbotin, R. I.; Maximov, A. Y.; Polshin, E. V.; Koposov, A. Y. *Dalton Trans.* **2007**, 3378−3389. (k) Rochford, J.; Rooney, A. D.; Pryce, M. T. *Inorg. Chem.* **2007**, *46*, 7247−7249. (l) Nemykin, V. N.; Galloni, P.; Floris, B.; Barrett, C. D.; Hadt, R. G.; Subbotin, R. I.; Marrani, A. G.; Zanoni, R.; Loim, N. M. *Dalton Trans.* **2008**, 4233−4246. (m) Nemykin, V. N.; Rohde, G. T.; Barrett, C. D.; Hadt, R. G.; Bizzarri, C.; Galloni, P.; Floris, B.; Nowik, I.; Herber, R. H.; Marrani, A. G.; Zanoni, R.; Loim, N. M. *J. Am. Chem. Soc.* **2009**, *131*, 14969−14978. (n) Galloni, P.; Floris, B.; de Cola, L.; Cecchetto, E.; Williams, R. M. *J. Phys. Chem. C* **2007**, *111*, 1517−1523. (o) Nemykin, V. N.; Rohde, G. T.; Barrett, C. D.; Hadt, R. G.; Sabin, J. R.; Reina, G.; Galloni, P.; Floris, B. *Inorg. Chem.* **2010**, *49*, 7497−7509. (p) Nemykin, V., N.; Hadt, R. G. *J. Phys. Chem. A* **2010**, *114*, 12062−12066. (q) Rohde, G. T.; Sabin, J. R.; Barrett, C. D.; Nemykin, V. N. *New J. Chem.* **2011**, *35*, 1440−1448. (r) Solntsev, P. V.; Neisen, B. D.; Sabin, J. R.; Gerasimchuk, N. N.; Nemykin, V. N. *J. Porphyrins Phthalocyanines* **2011**, *15*, 612−621. (s) Vecchi, A.; Gatto, E.; Floris, B.; Conte, V.; Venanzi, M.; Nemykin, V. N.; Galloni, P. *Chem. Commun.* **2012**, *48*, 5145−5147.

(7) (a) Sharma, R.; Gautam, P.; Mobin, S. M.; Misra, R. *Dalton Trans.* **2013**, *42*, 5539−5545. (b) Pareek, Y.; Ravikanth, M. *J. Organomet. Chem.* **2013**, *724*, 67−74. (c) Samanta, S.; Mittra, K.; Sengupta, K.; Chatterjee, S.; Dey, A. *Inorg. Chem.* **2013**, *52*, 1443−1453. (d) Devillers, C. H.; Milet, A.; Moutet, J.-C.; Pecaut, J.; Royal, G.; Saint-Aman, E.; Bucher, C. *Dalton Trans.* **2013**, *42*, 1196−1209. (e) Osipova, E. Yu.; Rodionov, A. N.; Simenel, A. A.; Belousov, Y. A.; Nikitin, O. M.; Kachala, V. V. *J. Porphyrins Phthalocyanines* **2012**, *16*, 1225−1232. (f) Nemykin, V. N.; Chen, P.; Solntsev, P. V.; Purchel, A. A.; Kadish, K. M. *J. Porphyrins Phthalocyanines* **2012**, *16*, 793−801. (g) Bakar, M. A.; Sergeeva, N. N.; Juillard, T.; Senge, M. O. *Organometallics* **2011**, *30*, 3225−3228. (h) Lyons, D. M.; Mohanraj, J.; Accorsi, G.; Armaroli, N.; Boyd, P. D. W. *New J. Chem.* **2011**, *35*, 632−639. (i) Subbaiyan, N. K.; Wijesinghe, C. A.; D'Souza, F. *J. Am. Chem. Soc.* **2009**, *131*, 14646−14647.

(8) (a) Burrell, A. K.; Campbell, W.; Officer, D. L. *Tetrahedron Lett.* **1997**, *38*, 1249−1252. (b) Burrell, A. K.; Campbell, W. M.; Officer, D. L.; Scott, S. M.; Gordon, K. C.; McDonald, M. R. *J. Chem. Soc., Dalton Trans.* **1999**, 3349−3354. (c) Jiao, L.; Courtney, B. H.; Fronczek, F. R.; Smith, K. M. *Tetrahedron Lett.* **2006**, *47*, 501−504. (d) Wang, H. J. H.; Jaquinod, L.; Olmstead, M. M.; Vicente, M. G. H.; Kadish, K. M.; Ou, Z.; Smith, K. M. *Inorg. Chem.* **2007**, *46*, 2898−2913. (e) Gryko, D. T.; Zhao, F.; Yasseri, A. A.; Roth, K. M.; Bocian, D. F.; Kuhr, W. G.; Lindsey, J. S. *J. Org. Chem.* **2000**, *65*, 7356−7362. (f) Schmidt, E. S.; Calderwood, T. S.; Bruice, T. C. *Inorg. Chem.* **1986**, *25*, 3718−3720. (g) Cheng, K.-L.; Li, H.-W.; Ng, D. K. P. *J. Organomet. Chem.* **2004**, *689*, 1593−1598. (h) Giasson, R.; Lee, E. J.; Zbao, X.; Wrighton, M. S. *J. Phys. Chem.* **1993**, *97*, 2596−2601. (i) Muraoka, T.; Kinbara, K.; Aida, T. *Nature* **2006**, *440*, 512−515.

(9) (a) Maiya, G. B.; Barbe, J. M.; Kadish, K. M. *Inorg. Chem.* **1989**, *28*, 2524−2527. (b) Solntsev, P. V.; Sabin, J. R.; Dammer, S. J.; Gerasimchuk, N. N.; Nemykin, V. N. *Chem. Commun.* **2010**, *46*, 6581−6583. (c) Kadish, K. M.; Xu, Q. Y.; Barbe, J. M. *Inorg. Chem.* **1987**, *26*, 2565−2566. (d) Xu, Q. Y.; Barbe, J. M.; Kadish, K. M. *Inorg. Chem.* **1988**, *27*, 2373−2378.

(10) (a) Vecchi, A.; Galloni, P.; Floris, B.; Nemykin, V. N. *J. Porphyrins Phthalocyanines* **2013**, *17*, 165−196. (b) Suijkerbuijk, B. M. J. M.; Klein Gebbink, R. J. M. *Angew. Chem., Int. Ed.* **2008**, *47*, 7396−7421.

(11) (a) Wang, C.-L.; Zhang, W.-B.; Yu, X.; Yue, K.; Sun, H.-J.; Hsu, C.-H.; Hsu, C.-S.; Joseph, J.; Modarelli, D. A.; Cheng, S. Z. D. *Chem.—Asian J.* **2013**, *8*, 947−955. (b) Konev, A. S.; Khlebnikov, A. F.; Nikiforova, T. G.; Virtsev, A. A.; Frauendorf, H. *J. Org. Chem.* **2013**, *78*, 2542−2552. (c) Frey, J.; Kodis, G.; Straight, S. D.; Moore, T. A.;

Moore, A. L.; Gust, D. *J. Phys. Chem. A* **2013**, *117*, 607−615. (d) El-Khouly, M. E.; Wijesinghe, C. A.; Nesterov, V. N.; Zandler, M. E.; Fukuzumi, S.; D'Souza, F. *Chem.—Eur. J.* **2012**, *18*, 13844−13853. (e) D'Souza, F.; Amin, A. N.; El-Khouly, M. E.; Subbaiyan, N. K.; Zandler, M. E.; Fukuzumi, S. *J. Am. Chem. Soc.* **2012**, *134*, 654−664. (f) Ciammaichella, A.; Dral, P. O.; Clark, T.; Tagliatesta, P.; Sekita, M.; Guldi, D. M. *Chem.—Eur. J.* **2012**, *18*, 14008−14016. (g) de Miguel, G.; Wielopolski, M.; Schuster, D. I.; Fazio, M. A.; Lee, O. P.; Haley, C. K.; Ortiz, A. L.; Echegoyen, L.; Clark, T.; Guldi, D. M. *J. Am. Chem. Soc.* **2011**, *133*, 13036−13054.

(12) (a) Bui, P. T.; Nishino, T.; Yamamoto, Y.; Shiigi, H. *J. Am. Chem. Soc.* **2013**, *135*, 5238−5241. (b) Kamimura, T.; Ohkubo, K.; Kawashima, Y.; Nobukuni, H.; Naruta, Y.; Tani, F.; Fukuzumi, S. *Chem. Science* **2013**, *4*, 1451−1461. (c) Yang, H.; Wang, Z.; Jin, H.; Hong, B.; Liu, Z.; Beavers, C. M.; Olmstead, M. M.; Balch, A. L. *Inorg. Chem.* **2013**, *52*, 1275−1284. (d) Konarev, D. V.; Zorina, L. V.; Khasanov, S. S.; Lyubovskaya, R. N. *Dalton Trans.* **2012**, *41*, 9170−9175. (e) Konarev, D. V.; Khasanov, S. S.; Faraonov, M. A.; Lyubovskaya, R. N. *CrystEngComm* **2012**, *14*, 4350−4356. (f) Yang, H.; Jin, H.; Zhen, H.; Wang, Z.; Liu, Z.; Beavers, C. M.; Mercado, B. Q.; Olmstead, M. M.; Balch, A. L. *J. Am. Chem. Soc.* **2011**, *133*, 6299−6306. (g) Mercado, B. Q.; Stuart, M. A.; Mackey, M. A.; Pickens, J. E.; Confait, B. S.; Stevenson, S.; Easterling, M. L.; Valencia, R.; Rodriguez-Fortea, A.; Poblet, J. M. *J. Am. Chem. Soc.* **2010**, *132*, 12098−12105. (h) D'Souza, F.; Deviprasad, G. R.; Zandler, M. E.; Rath, N. P. *Chem. Commun.* **2001**, 267−268. (i) Wilson, S. R.; MacMahon, S.; Tat, F. T.; Jarowski, P. D.; Schuster, D. I. *Chem. Commun.* **2003**, 226−227. (j) Zhang, S.; Echegoyen, L. *Tetrahedron* **2006**, *62*, 1947−1954.

(13) (a) Zhao, H.; Zhu, Y.; Chen, C.; He, L.; Zheng, J. *Carbon* **2012**, *50*, 4894−4902. (b) Lee, S.-H.; Larsen, A. G.; Ohkubo, K.; Cai, Z.-L.; Reimers, J. R.; Fukuzumi, S.; Crossley, M. J. *Chem. Sci.* **2012**, *3*, 257−269. (c) Poddutoori, P. K.; Sandanayaka, A. S. D.; Hasobe, T.; Ito, O.; van der Est, A. *J. Phys. Chem. B* **2010**, *114*, 14348−14357. (d) Mateo-Alonso, A.; Prato, M. *Eur. J. Org. Chem.* **2010**, 1324−1332. (e) Spaenig, F.; Kovacs, C.; Hauke, F.; Ohkubo, K.; Fukuzumi, S.; Guldi, D. M.; Hirsch, A. *J. Am. Chem. Soc.* **2009**, *131*, 8180−8195. (f) Winters, M. U.; Dahlstedt, E.; Blades, H. E.; Wilson, C. J.; Frampton, M. J.; Anderson, H. L.; Albinsson, B. *J. Am. Chem. Soc.* **2007**, *129*, 4291−4297. (g) Schmittel, M.; Kishore, R. S. K.; Bats, J. W. *Org. Biomol. Chem.* **2007**, *5*, 78−86. (h) D'Souza, F.; Chitta, R.; Gadde, S.; Islam, D.-M. S.; Schumacher, A. L.; Zandler, M. E.; Araki, Y.; Ito, O. *J. Phys. Chem. B* **2006**, *110*, 25240−25250.

(14) Zhu, P.; Zhang, X.; Wang, H.; Zhang, Y.; Bian, Y.; Jiang, J. *Inorg. Chem.* **2012**, *51*, 5651−5659.

(15) (a) Rieke, R. D.; Chao, L. C. *J. Org. Chem.* **1975**, *40*, 2253−2255. (b) Tabard, A.; Guilard, R.; Kadish, K. M. *Inorg. Chem.* **1986**, *25*, 4277−4285. (c) Krivokapic, A.; Anderson, H. L.; Bourhill, G.; Ives, R.; Clark, S.; McEwan, K. J. *Adv. Mater.* **2001**, *13*, 652−656.

(16) Chen, C.-Y.; Sun, E.; Fan, D.; Taniguchi, M.; McDowell, B. E.; Yang, E.; Diers, J. R.; Bocian, D. F.; Holten, D.; Lindsey, J. S. *Inorg. Chem.* **2012**, *51*, 9443−9464.

(17) Parzuchowski, P. G.; Kampf, J. W.; Rozniecka, E.; Kondratenko, Y.; Malinowska, E.; Meyerhoff, M. E. *Inorg. Chim. Acta* **2003**, *355*, 302−313.

(18) Ball, R. G.; Lee, K. M.; Marshall, A. G.; Trotter, J. *Inorg. Chem.* **1980**, *19*, 1463−1469.

(19) Bedel-Cloutour, C. H.; Mauclaire, L.; Pereyre, M.; Adams, S.; Drager, M. *Polyhedron.* **1990**, *9*, 1297−1303.

(20) Raptopoulou, C.; Daphnomili, D.; Karamalides, A.; Vaira, M. D.; Terzis, A.; Coutsolelos, A. G. *Polyhedron.* **2004**, *23*, 1777−1784.

(21) Lecomte, C.; Protas, J.; Cocolios, P.; Guilard, R. *Acta Crystallogr., Sect.B: Struct. Crystallogr. Cryst. Chem.* **1980**, *36*, 2769−2771.

(22) Eaton, S. S.; Eaton, G. R. *J. Am. Chem. Soc.* **1975**, *97*, 3660−3666.

(23) (a) Barriere, F.; Geiger, W. E. *J. Am. Chem. Soc.* **2006**, *128*, 3980−3989. (b) Geiger, W. E.; Connelly, N. G. *Adv. Organomet. Chem.* **1985**, *24*, 87−130.

(24) (a) D'Alessandro, D. M.; Keene, F. R. *Dalton Trans.* **2004**, 3950−3954. (b) D'Alessandro, D.; Keene, R. *Chem. Soc. Rev.* **2006**, *35*, 424−440.

(25) Robin, M. B.; Day, P. *Adv. Inorg. Chem. Radiochem.* **1967**, *10*, 247−422.

(26) (a) Hush, N. S. *Prog. Inorg. Chem.* **1967**, *8*, 391−444. (b) Creutz, C. *Prog. Inorg. Chem.* **1983**, *30*, 1−73. (c) Hush, N. S. *Coord. Chem. Rev.* **1985**, *64*, 135−157.

(27) (a) Solntsev, P. V.; Dudkin, S. V.; Sabin, J. R.; Nemykin, V. N. *Organometallics* **2011**, *30*, 3037−3046. (b) Hildebrandt, A.; Lehrich, S. W.; Schaarschmidt, D.; Jaeschke, R.; Schreiter, K.; Spange, S.; Lang, H. *Eur. J. Inorg. Chem.* **2012**, *2012*, 1114−1121. (c) Hildebrandt, A.; Schaarschmidt, D.; Claus, R.; Lang, H. *Inorg. Chem.* **2011**, *50*, 10623−10632. (d) Hildebrandt, A.; Schaarschmidt, D.; Lang, H. *Organometallics* **2011**, *30*, 556−563.

(28) Gouterman, M. *J. Mol. Spectrosc.* **1961**, *6*, 138−163.

(29) (a) Masson, E. *Org. Biomol. Chem.* **2013**, *11*, 2859−2871. (b) Pandith, A. H.; Islam, N.; Syed, Z. F.; Rehman, S.-U.; Bandaru, S.; Anoop, A. *Chem. Phys. Lett.* **2011**, *516*, 199−203. (c) Paul, B.; Butterfoss, G. L.; Boswell, M. G.; Renfrew, P. D.; Yeung, F. G.; Shah, N. H.; Wolf, C.; Bonneau, R.; Kirshenbaum, K. *J. Am. Chem. Soc.* **2011**, *133*, 10910−10919. (d) Talotta, C.; Gaeta, C.; Troisi, F.; Monaco, G.; Zanasi, R.; Mazzeo, G.; Rosini, C.; Neri, P. *Org. Lett.* **2010**, *12*, 2912−2915. (e) Lunazzi, L.; Mancinelli, M.; Mazzanti, A. *J. Org. Chem.* **2009**, *74*, 1345−1348. (f) Pietra, F. *J. Phys. Org. Chem.* **2007**, *20*, 1102−1107. (g) Ceccacci, F.; Mancini, G.; Mencarelli, P.; Villani, C. *Tetrahedron: Asymmetry* **2003**, *14*, 3117−3122.

(30) Crane, J. D.; Hitchcock, P. B.; Kroto, H. W.; Taylor, R.; Walton, D. R. M. *Chem. Commun.* **1992**, *24*, 1764−5.

(31) Frisch, M. J.; Trucks, G. W.; Schlegel, H. B.; Scuseria, G. E.; Robb, M. A.; Cheeseman, J. R.; Montgomery, Jr., J. A.; Vreven, T.; Kudin, K. N.; Burant, J. C.; Millam, J. M.; Iyengar, S. S.; Tomasi, J.; Barone, V.; Mennucci, B.; Cossi, M.; Scalmani, G.; Rega, N.; Petersson, G. A.; Nakatsuji, H.; Hada, M.; Ehara, M.; Toyota, K.; Fukuda, R.; Hasegawa, J.; Ishida, M.; Nakajima, T.; Honda, Y.; Kitao, O.; Nakai, H.; Klene, M.; Li, X.; Knox, J. E.; Hratchian, H. P.; Cross, J. B.; Adamo, C.; Jaramillo, J.; Gomperts, R.; Stratmann, R. E.; Yazyev, O.; Austin, A. J.; Cammi, R.; Pomelli, C.; Ochterski, J. W.; Ayala, P. Y.; Morokuma, K.; Voth, G. A.; Salvador, P.; Dannenberg, J. J.;. Zakrzewski, V. G.; Dapprich, S.; Daniels, A. D.; Strain, M. C.; Farkas, O.; Malick, D. K.; Rabuck, A. D.; Raghavachari, K.; Foresman, J. B.; Ortiz, J. V.; Cui, Q.; Baboul, A. G.; Clifford, S.;. Cioslowski, J.; Stefanov, B. B.; Liu, G.;. Liashenko, A.; Piskorz, P.; Komaromi, I.; Martin, R. L.; Fox, D. J.; Keith, T.; Al-Laham, M. A.; Peng, C. Y.; Nanayakkara, A.; Challacombe, M.; Gill, P. M. W.; Johnson, B.; Chen, W.; Wong, M. W.; Gonzalez, C.; Pople, J. A. *Gaussian 03*, Revision C.02; Gaussian, Inc.: Wallingford, CT, 2004.

(32) Nemykin,V. N.; Basu, P. *VMOdes Program*, Revision A 7.2; University of Minnesota Duluth: Duluth, MN and Duquesne University: Pittsburgh, PA, 2001, 2003, 2005.

(33) (a) Becke, A. D. *Phys. Rev. A* **1988**, *38*, 3098−3100. (b) Perdew, J. P. *Phys. Rev. B* **1986**, *33*, 8822−8824.

(34) (a) Zhang, L.; Qi, D.; Zhang, Y.; Bian, Y.; Jiang, J. *J. Mol. Graphics Modell.* **2011**, *29*, 717−725. (b) Herber, R. H.; Nowik, I.; Grosland, J. O.; Hadt, R. G..; Nemykin, V. N. *J. Organomet. Chem.* **2008**, *693*, 1850−1856. (c) Nemykin, V. N.; Makarova, E. A.; Grosland, J. O.; Hadt, R. G.; Koposov, A. Y. *Inorg. Chem.* **2007**, *46*, 9591−9601. (d) Nemykin, V. N.; Maximov, A. Y.; Koposov, A. Y. *Organometallics* **2007**, *26*, 3138−3148. (e) Nemykin, V. N.; Olsen, J. G.; Perera, E.; Basu, P. *Inorg. Chem.* **2006**, *45*, 3557−3568. (f) Nemykin, V. N.; Hadt, R. G. *Inorg. Chem.* **2006**, *45*, 8297−8307. (g) Li, Y. L.; Han, L.; Mei, Y.; Zhang, J. Z. H. *Chem. Phys. Lett.* **2009**, *482*, 217−222. (h) Fabrizi de Biani, F.; Manca, G.; Marchetti, L.; Leoni, P.; Bruzzone, S.; Guidotti, C.; Atrei, A.; Albinati, A.; Rizzato, S. *Inorg. Chem.* **2009**, *48*, 10126−10137. (i) Li, F.; Sa, R.; Wu, K. *Mol. Phys.* **2008**, *106*, 2537−2544. (j) Santi, S.; Orian, L.; Donoli, A.; Durante, C.; Bisello, A.; Ganis, P.; Ceccon, A.; Crociani, L.; Benetollo, F. *Organometallics* **2007**, *26*, 5867−5879. (k) Zhang, W.-W.; Yu, Y.-G.; Lu, Z.-D.; Mao, W.-L.; Li, Y.-Z.; Meng, Q.-J. *Organometallics* **2007**, *26*,

865−873. (l) Parac, M.; Grimme, S. *J. Phys. Chem. A* **2002**, *106*, 6844−6850. (m) Solntsev, P. V.; Spurgin, K. L.; Sabin, J. R.; Heikal, A. A.; Nemykin, V. N. *Inorg. Chem.* **2012**, *51*, 6537−6547.
(35) (a) Becke, A. D. *J. Chem. Phys.* **1993**, *98*, 5648−5652. (b) Lee, C.; Yang, W.; Parr, R. G. *Phys. Rev. B* **1988**, *37*, 785−789.
(36) Adamo, C.; Barone, V. *J. Chem. Phys.* **1999**, *110*, 6158−6169.
(37) Wachters, A. J. H. *J. Chem. Phys.* **1970**, *52*, 1033.
(38) Godbout, N.; Salahub, D. R.; Andzelm, J.; Wimmer, E. *Can. J. Chem.* **1992**, *70*, 560−571.
(39) McLean, A. D.; Chandler, G. S. *J. Chem. Phys.* **1980**, *72*, 5639−5648.
(40) Hay, P. J.; Wadt, W. R. *J. Chem. Phys.* **1985**, *82*, 299−310.
(41) Altomare, A.; Cascarano, G.; Giacovazzo, C.; Guagliardi, A.; Burla, M. C.; Polidori, G.; Camalli, M. J. *Appl. Crystallogr.* **1994**, *27*, 435.
(42) Sheldrick, G. M. *Acta Crystallogr.* **2008**, *A64*, 112.
(43) Spek, A. L. *Acta Crystallogr.* **2009**, *D65*, 148−155.
(44) Burnett, M. N.; Johnson, C. K. *ORTEP-III: Oak Ridge Thermal Ellipsoid Plot Program for Crystal Structure Illustrations*, Oak Ridge National Laboratory Report ORNL-6895; Oak Ridge National Laboratory: Oak Ridge, TN, 1996.

dx.doi.org/10.1021/ic401163y | *Inorg. Chem.* 2013, 52, 9496−9510